RECLAMATION

Managing Water in the West

Desalination and Water Purification Research and Development Program Report No. 99

Novel Membrane and Device for Direct Contact Membrane Distillation-Based Desalination Process: Phase III

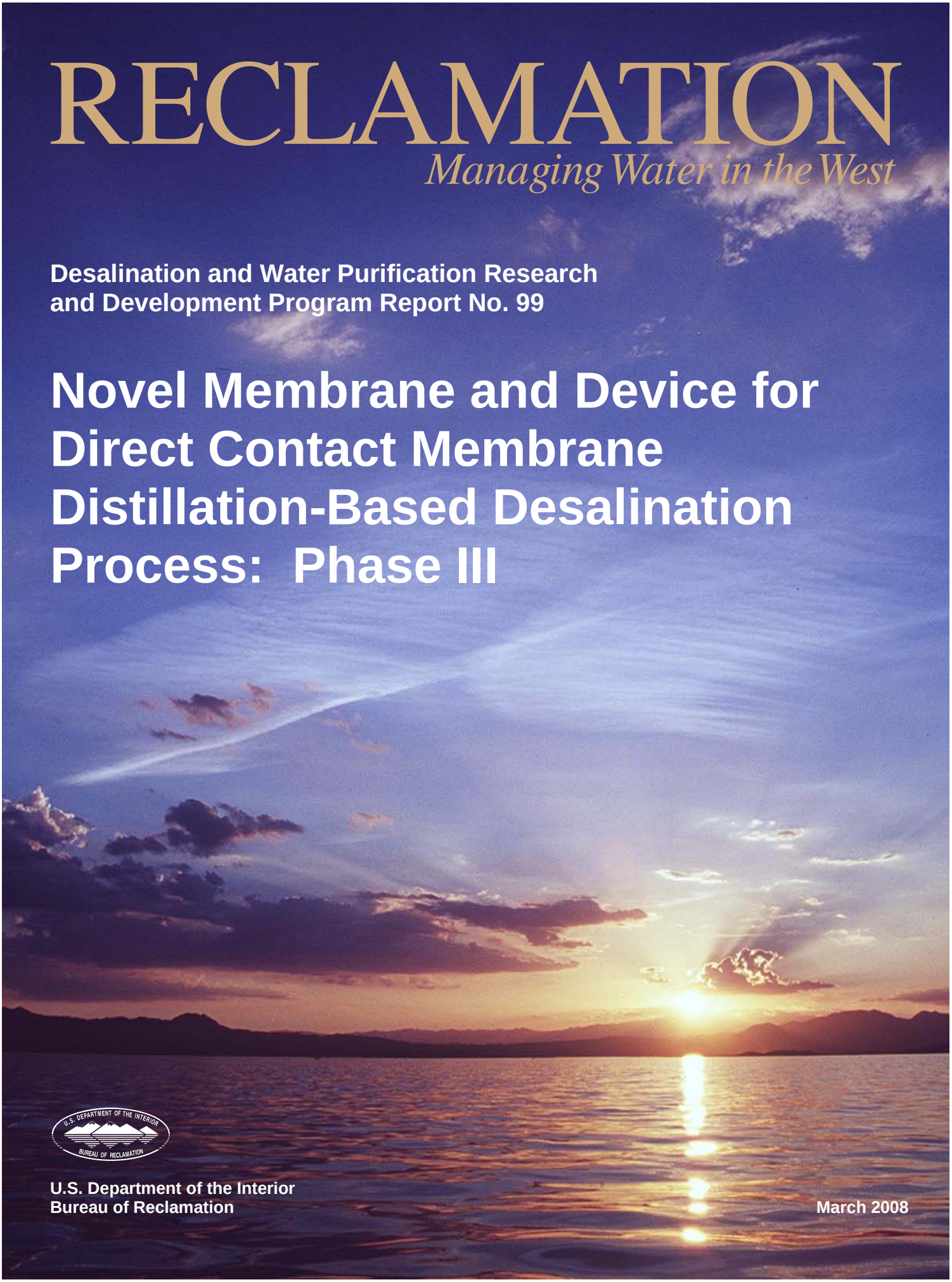

U.S. Department of the Interior
Bureau of Reclamation

March 2008

REPORT DOCUMENTATION PAGE

Form Approved
OMB No. 0704-0188

1. REPORT DATE *(DD-MM-YYYY)*	2. REPORT TYPE	3. DATES COVERED *(From - To)*
March 2008	Final	October 2002 - May 2005

4. TITLE AND SUBTITLE
Novel Membrane and Device for Direct Contact Membrane Distillation-Based Desalination Process: Phase III

5a. CONTRACT NUMBER
02-FC-81-0840

5b. GRANT NUMBER

5c. PROGRAM ELEMENT NUMBER

6. AUTHOR(S)
K.K.Sirkar and Baoan Li

5d. PROJECT NUMBER

5e. TASK NUMBER
Task A

5f. WORK UNIT NUMBER

7. PERFORMING ORGANIZATION NAME(S) AND ADDRESS(ES)
New Jersey Institute of Technology
Center for Membrane Technologies
Room 362 Tiernan Hall
323 Dr. King Blvd Newark, NJ 07102

8. PERFORMING ORGANIZATION REPORT NUMBER

9. SPONSORING / MONITORING AGENCY NAME(S) AND ADDRESS(ES)
U.S. Department of the Interior
Bureau of Reclamation,
Denver Federal Center
PO Box 25007, Denver CO 80225-0007

10. SPONSOR/MONITOR'S ACRONYM(S)

11. SPONSOR/MONITOR'S REPORT NUMBER(S)
DWPR Report No. 99

12. DISTRIBUTION / AVAILABILITY STATEMENT
Available from the National Technical Information Service (NTIS), Operations Division, 5285 Port Royal Road, Springfield VA 22161

13. SUPPLEMENTARY NOTES
Report can be downloaded from Reclamation Web site:
www.usbr.gov/pmts/water/publications/reports.html

14. ABSTRACT ***(Maximum 200 words)***

Phase III project on novel membrane and device for direct contact membrane distillation (DCMD) based desalination scaled up the hollow-fiber membrane surface area in the module successfully studied in Phase II by more than an order of magnitude to 0.29 m^2 using 1088 hollow fibers having a plasmapolymerized coating recipe somewhat similar to that in Phase II module MXFR #3. The packing fraction of 25.4-cm long fibers was 0.22. Brine feed temperature ranged between 40 and 94 ^oC; a high water vapor flux of 60 $kg/m^2 \cdot h$ was achieved at 90 ^oC in module S/N 1004 at reasonable brine cross flow velocities (Reynolds number, Re, 78). Since Re values were similar to those in much smaller Phase II modules, module/process scale-up was successful. An extended-term 128 hour-long DCMD test using 87-90 ^oC brine prefiltrated with 1 micron microfiltration unit yielded a steady flux of 54 $kg/m^2 \cdot h$; the flux decayed only 6% from the initial value. Modules S/N 1004 and S/N 1005 were stacked back-to-back to demonstrate further scaleup. Studies using 3%, 6%, and 10% brines indicated limited flux drop suggesting DCMD for brine concentrate volume reduction. Estimated cost of water by DCMD was much less than that by reverse osmosis.

15. SUBJECT TERMS
direct contact membrane distillation (DCMD), porous polypropylene hollow fibers, microporous silicone-fluoropolymer coating, desalination, cross-flow modules, scale-up

16. SECURITY CLASSIFICATION OF:			17. LIMITATION OF ABSTRACT	18. NUMBER OF PAGES	19a. NAME OF RESPONSIBLE PERSON
a. REPORT	b. ABSTRACT	c. THIS PAGE			Frank Leitz
UL	UL	UL	SAR	77	19b. TELEPHONE NUMBER *(include area code)* 303-445-2255

Desalination and Water Purification Research and Development Program Report No. 99

Novel Membrane and Device for Direct Contact Membrane Distillation-Based Desalination Process: Phase III

Prepared for Reclamation Under Agreement No. 02-FC-81-0840

By

Dr. Kamalesh K. Sirkar
Dr. Baoan Li

New Jersey Institute of Technology
Newark, New Jersey

U.S. Department of the Interior
Bureau of Reclamation
Technical Service Center
Water and Environmental Services Division
Water Treatment Engineering Research Team
Denver, Colorado

March 2008

MISSION STATEMENTS

The mission of the Department of the Interior is to protect and provide access to our Nation's natural and cultural heritage and honor our trust responsibilities to Indian tribes and our commitments to island communities.

The mission of the Bureau of Reclamation is to manage, develop, and protect water and related resources in an environmentally and economically sound manner in the interest of the American public.

Acknowledgments

The research conducted under this contract was sponsored by Desalination and Water Purification Research and Development Program, Bureau of Reclamation, Denver, Colorado.

Disclaimer

The views, analysis, recommendations, and conclusions in this report are those of the authors and do not represent official or unofficial policies or opinions of the United States Government, and the United States takes no position with regard to any findings, conclusions, or recommendations made. As such, mention of trade names or commercial products does not constitute their endorsement by the United States Government.

Table of Contents

List of Tables

List of Figures

Figure

Glossary

a_i	activity coefficient of i in solution
A_r	membrane area ratio for heat transfer through a membrane surface
A_{rf}	value of A_r for hot brine-membrane interface, d_o / d_i
$A_{r\ln}$	value of A_r for logarithmic mean membrane area, $d_{r\ln} / d_i$, where logarithmic mean diameter, $d_{r\ln} = (d_o - d_i) / \ln(d_o / d_i)$
A_{rp}	value of A_r for cold distillate- membrane interface, d_i / d_i, which is equal to 1
cm	centimeter
cm/min	centimeters per minute
cm^2	square centimeter(s)
^oC	degrees Celsius
c	bulk liquid phase molar concentration of water
c_p	liquid heat capacity
C	salt concentration
d	fiber inside or outside diameter
d_i	fiber inside diameter (I.D.)
d_o	fiber outside diameter (O.D.)
D	characteristic dimension
D_{AB}	ordinary diffusion coefficient of solute in water
DCMD	direct contact membrane distillation
$/m^2	dollars per square meter
$/gal/day	dollars per gallon per day
$/kgal	dollars per thousand gallons

DI	deionized
F	water vapor flux
F_c	tube-row correction factor
gpm	gallons per minute
h	overall boundary layer heat transfer coefficient
h_c	effective membrane heat transfer coefficient
h_f	shell side boundary layer heat transfer coefficient
h_{mg}	heat transfer coefficient of the vapor/gas within the membrane pores
h_{ms}	heat transfer coefficient of the solid polymeric membrane material
h_m	membrane heat transfer coefficient
h_p	tube side boundary layer heat transfer coefficient
h_v	heat transfer coefficient related to the water vapor flux
hr	hour
H	Henry's Law constant for water
Hg	mercury
I.D.	internal diameter
k	liquid thermal conductivity
kgal	thousand gallons
kg/m2•h	kilograms per square meter hour
k_f	mass transfer coefficient for hot brine feed
k_m	mass transfer coefficient for membrane
k_p	mass transfer coefficient for cold distillate
K	overall mass transfer coefficient

kg	kilogram
kW	kilowatt
L	fiber length
L/min	liters per minute
m	meter
m^2	square meter
m^3/day	cubic meters per day
m^3/s	cubic meters per second
MD	membrane distillation
mg/L	milligrams per liter
min	minute(s)
n	number of fibers in a membrane module
N_2	nitrogen
NaCl	sodium chloride
Nu	Nusselt number
N_V	mass flux of water vapor across the membrane
O.D.	outside diameter
%	percent
p_{fm}	water vapor partial pressure at hot brine-membrane interface
p_{pm}	water vapor partial pressure at cold distillate-membrane interface
p_i^0	saturation pressure of pure i
p_{water}^o	saturation pressure of water
P_1	atmospheric pressure
PP	polypropylene

ppm	parts per million
Pr	Prandtl number
Pr_w	Prandtl number evaluated at the tube-wall temperature
psi	pounds per square inch
psig	pounds per square inch gage
Q	effective heat flux through the membrane
Q_{N_2}	permeability coefficient of N_2 permeation through the membrane of effective thickness δ_M
Q_{N_2}/δ_M	N_2 permeance
Q_m	heat flux conducted through the nonporous solid polymeric part of the membrane and the gas phase that fills the pores
Q_V	heat flux transferred by vapor flux across the membrane
Re	Reynolds Number
Re_d	diameter-based Reynolds number
RO	reverse osmosis
s	inside membrane area ($= n\pi d_i L$)
Sc	Schmidt number
Sh	Sherwood number
STP	T_0 = 273.15 K, P_0 = 760 Torr
T	temperature
TBRDC	Tularosa Basin Research and Development Center
TDS	total dissolved solids
T_1	room temperature
T_f	bulk temperature of feed

T_{fm}	interface temperature on the surface of membrane in feed side
T_{fm}/T_f	degree of temperature polarization in VMD
TPC	temperature polarization coefficient
μm	micrometer
u	constant
U	overall heat transfer coefficient of DCMD process
V	velocity
V_{feed}	volumetric flow rate of the feed
V_I	interstitial velocity of liquid flowing on the shell side of fibers in rectangular cross flow membrane module
V_1	volumetric flow rate of gas through the membrane at room temperature
V_L	linear velocity of liquid flowing on the tube side of fibers
VMD	vacuum membrane distillation
W/m^2K	watts per square meter Kelvin
W/m·K	watts per meter Kelvin
x	solute mole fraction
x_f	solute mole fraction in the bulk feed
x_{fm}	solute mole fraction at the membrane surface
x_i	liquid mole fraction of species i, water
x_{NaCl}	mole fraction of NaCl in water solution
x_p	solution concentration (mole fraction) in the permeate
y_i	vapor mole fraction of water
ρ	density

μ	dynamic viscosity (absolute viscosity)
μ_W	liquid viscosity evaluated at the tube-wall temperature
η	membrane heat transfer efficiency
δ_M	effective thickness of membrane
ε	membrane porosity
ΔH_V	heat of vaporization of water
Δp_m	water vapor pressure difference across the membrane, DCMD driving force
ΔP_{N_2}	N_2 pressure difference across the membrane
ΔT	bulk temperature difference between feed and distillate ($T_f - T_p$)
ΔT_f	temperature drop of feed along the module length
ΔT_F	temperature difference between brine bulk temperature and the temperature of brine-membrane interface on the feed side
ΔT_m	trans-membrane temperature difference
ΔT_P	the temperature difference between the temperature of membrane-distillate interface and distillate bulk temperature on distillate side

1. Executive Summary

Although research and development studies to improve commercialized reverse osmosis and thermally-driven desalination processes are continuing, there exists a need to develop and evaluate alternate desalination technologies, e.g., membrane distillation (MD), which utilizes waste heat. In one variety of MD, direct contact membrane distillation (DCMD), hot brine flows on one side of a gas-filled porous hydrophobic hollow-fiber membrane and cold distillate flows on the other side of the membrane. This technique is of interest here. The primary deficiencies of this technique are flux reduction due to long-term pore wetting and reduced brine-side heat and mass transfer coefficients.

To overcome these deficiencies, a number of changes were introduced in Phase II of this research on the DCMD process (Sirkar and Li, 2003): (1) the porous hydrophobic hollow-fiber membrane had a thin water-vapor-permeable hydrophobic microporous coating of a silicone-fluoropolymer plasmapolymerized on the fiber outside diameter on the hot brine side to prevent pore wetting; (2) to increase the brine-side heat transfer coefficient drastically, the hot brine feed was in a rectangular crossflow mode vis-à-vis the hollow-fiber membranes; (3) the hydrophobic porous hollow fibers had thick walls and high porosity; (4) the module design ensured that the temperature rise of the cold distillate was minimal. Extensive data obtained in Phase II indicated a stable and a highly productive DCMD process with water vapor fluxes reaching as high as 79 kilograms per square meter hour ($kg/m^2 \cdot h$) at 90 ^oC in the module MXFR #3 having a membrane surface area of 119 square centimeters (cm^2).

The present Phase III project has scaled up the membrane surface area by more than an order of magnitude using the same porous hydrophobic polypropylene hollow-fiber membranes (internal diameter 330 micrometers (μm), wall thickness 150 μm) as in Phase II. These fibers had a plasmapolymerized microporous coating of a silicone-fluoropolymer close to that of the module MXFR #3. In the rectangular crossflow module design, the number of fibers in a module was 1,088. The membrane surface area in each module was 2,864 cm^2. The brine feed temperature ranged from 40-94 degrees Celsius (^oC) in DCMD. At a high-feed velocity over the fibers, a water permeation flux as high as 60 $kg/m^2 \cdot h$ was achieved in DCMD at 90 ^oC through the module S/N 1004. Such a flux value is similar to that achieved in an order of magnitude smaller module MXFR #3 of Phase II. Further, the Reynolds number of brine was in the range used in Phase II. This indicated that, using appropriate fibers and a reasonable crossflow velocity on the shell side, the desired water permeation flux can be obtained regardless of the scale of operation. No leakage of salt or water was encountered during the extended use of this module in DCMD.

Nitrogen permeation tests through different modules indicated that the fibers in the module S/N 1004 had significantly lower N_2 permeance than that in MXFR #3; this indicated that the coating on the outer surface of the hollow fiber was tighter than that on the fibers in MXFR #3. That is the reason why the water vapor flux of larger module S/N 1004 was somewhat smaller than that of the smaller module MXFR #3 of Phase II. An extended-term DCMD test was carried out for a period of 128 hours at a temperature of 87-90 ^{o}C using the module S/N 1004. The steady-state water vapor flux was found to be ~ 54 kg/m^2·h. This is quite close to the steady-state flux achieved in the long-term test in Phase II. The initial time flux decay (only 6 percent [%]) was likely to be due to a thermal creep in the coatings and a slight fouling on the surfaces of the fibers. The membrane pores were not wetted by the hot brine during the operation. The silicone-fluoropolymer coating provided an effective barrier to protect the membrane. The performance of a 2-module stack was also studied. The successful performance of the stack in this experiment illustrated how one can stack a number of the horizontal crossflow modules in a small volume and extract as much water vapor as possible from a given hot brine stream. Further studies with brines of higher salt concentration, e.g., 6% and 10%, indicated very limited flux reductions; the DCMD process may be useful for brine concentrate volume reduction.

2. Background and Introduction to Potential Solution

Research and development of desalination technologies to increase the availability of cheap and reliable sources of potable water is of significant importance due to the ever increasing population and their needs. Although research and development efforts have focused primarily on existing membrane-based and thermally-driven processes and technologies, there is need for alternative desalination technologies which may potentially be easier to use, cost effective and use energy like low-grade waste heat currently not utilized. Membrane distillation is one such process for desalination.

Membrane distillation (MD) is an evaporation process of a volatile solvent or solute species from a solution (in most cases, an aqueous solution), driven by a difference between its partial pressure over the solution contacting one side of a porous hydrophobic membrane and its partial pressure on the other side of the membrane. When the partial pressure difference through the membrane is created by the direct contacting of a liquid cooler than the feed on the other side of the membrane, the process is called direct contact membrane distillation (DCMD). This is illustrated for a hollow-fiber-based process in figure 1a where the hot brine flows on the shell side of the fiber and the cold distillate flows on the tube side through the fiber bore. When the side of the hollow-fiber membrane opposite to the hot brine is subjected to vacuum to develop a partial pressure difference across the membrane, the process is identified as vacuum membrane distillation (VMD). Figure 1b illustrates the VMD process where the hot brine flows on the shell side of the fiber and vacuum is applied on the tube side.

In an MD process, the membrane used must be porous and hydrophobic. Surface tension forces withhold liquids from the pores and prevent the penetration by the liquids and, thus, contact between the two liquids in a DCMD process. Generally, the solutions are aqueous and their surface tensions higher than the critical surface tension of the polymer making the membrane. In a DCMD process, the temperature difference, causing a corresponding vapor pressure difference across the membrane, provides the driving force of the membrane distillation process. Evaporation will occur at the solution surface if the vapor pressure on the solution side is greater than the vapor pressure at the condensate surface. Vapors then diffuse through the pores to the cooler surface where they condense. The dependences of mass and heat transport upon different membrane and process parameters involved in membrane distillation have been investigated theoretically (Schofield et al., 1987, 1990a, b; Lawson and Lloyd, 1996a; Martinez-Diez and Vazquez-Gonzalez, 1999).

A system of great research interest in MD is the production of fresh water from saline water. The advantages of membrane distillation for water production by such a method are:

(a) It produces high quality distillate.

(b) Water can be distilled at relatively low temperatures (30-100 degrees Celsius [ºC]) and low pressure (1 atmosphere [atm]).

(c) Low-grade heat (solar, industrial waste heat or desalination waste heat) may be used.

(d) The water may not require extensive pretreatment to prevent membrane fouling as in pressure-based membrane processes.

Potential disadvantages of the process are:

(a) The water evaporation rate is strongly controlled by the brine side heat transfer coefficient resulting in a relatively low permeate flux compared to other membrane filtration processes, such as reverse osmosis (RO).

(b) Over an extended time, there is flux decay and distillate contamination due to pore wetting.

(c) Economic costs are uncertain.

There are a number of ways to overcome the deficiencies. To prevent pore wetting and long-term flux decay, an extremely thin, highly water-vapor-permeable microporous coating of a hydrophobic silicone-fluoropolymer could be applied on the outside surface of the porous hydrophobic hollow fibers facing the hot brine to make the membrane essentially nonwettable. The resulting configuration for DCMD is illustrated in figure 1c. The corresponding configuration for VMD is shown in figure 1d. Secondly, transverse flow of hot brine over this coated fiber surface could be implemented via novel rectangular crossflow module designs to enhance the brine side heat transfer coefficient, reduce temperature polarization and thereby increase the water vapor flux across the membrane.

In Phase I of this project carried out earlier (Sirkar and Qin, 2001), modules having an ultrathin microporous silicone coating on the outside surface of hydrophobic porous polypropylene hollow fibers of smaller diameters were employed. Using a parallel flow Module 4 and high hot water velocity in the fiber bore (figure 1e) yielded a water flux of 15 $kg/m^2 \cdot h$ at 91 ^oC in VMD. There was no pore wetting during and after a cumulative experimental duration of 1,000 hours (hr) (among them approximately 400 hrs for 1% by weight (wt%) or

3 wt% brine) without any module washing in between the runs. The ultrathin plasmapolymerized silicone coating on the porous hollow-fiber surface was also successful in preventing any pore wetting by hot water or hot saline solutions when these solutions were flowing on the coating side. A large rectangular module having 6,000 microporous hollow fibers having an interior diameter (I.D.) of 200 micrometers (μm) and outside diameter (O.D.) of 305 μm (polypropylene [PP], Akzo) with an appropriate coating yielded very low water vapor flux in DCMD. Generally, the performance in DCMD for all modules studied was poor in the sense that the water vapor flux was quite low—in the range of 0.01-0.8 $kg/m^2 \cdot h$. It was observed that, for the system dimensions, the shell-side Reynolds number of hot brine achieved under the laboratory conditions was quite low. Further conductive heat loss was substantial. Moreover, the cold distillate temperature was too high at the exit. It meant that much higher cold distillate flow rate was needed to keep its temperature low.

In Phase II of this project (Sirkar and Li, 2003), the experimental research explored a number of approaches to radically enhance the actual DCMD process performance. The rectangular crossflow module design, the fiber packing, and the experimental flow conditions were such as to ensure the achievement of appropriately high Reynolds number in the shell-side crossflow of the hot brine. This reduced the temperature polarization on the brine side (figure 1f). Increased fiber bore diameter, decreased fiber number, and an appropriate distillate flow rate were employed to provide limited temperature rise in the cold distillate under moderate pressure drop. Six small hollow-fiber modules having rectangular crossflow of hot brine over the outside fiber diameter and cold distillate flow in the fiber bore were successfully studied for DCMD-based water recovery from hot feed brine over a temperature range of 60-90 °C. The fibers had a microporous plasmapolymerized coating of a silicone-fluoropolymer on the O.D. Under no circumstances did we encounter any salt leakage into the fiber bore distillate streams. Modules MXFR #1 and MXFR #3 employing PP 150/330 hollow fibers (330-μm I.D., 150-μm thickness) having very open microporous silicone-fluoropolymer coatings showed very high DCMD and VMD performances. Other modules employing smaller diameter fibers having less open coatings yielded much poorer performance in DCMD and VMD. A water vapor permeation flux of 79 $kg/m^2 \cdot h$ based on the fiber I.D. was achieved at 90 °C in DCMD in the module MXFR #3 with the hot brine in rectangular crossflow on the fiber O.D. and cold distillate in the fiber bore. Module MXFR #3 was used extensively for more than 400 hrs. This includes a continuous 5-day-long DCMD run with 85 °C brine containing 1 percent (%) sodium chloride (NaCl). A stable water flux of ~ 54 $kg/m^2 \cdot h$ was obtained. Such a high flux value was achieved due to the high heat transfer coefficient in the rectangular crossflow of brine, more open microporous silicone-fluoropolymer coating on the fiber O.D., thicker fiber wall reducing conductive heat loss, and a

lower cold distillate temperature rise due to higher distillate flow rate in the larger diameter fiber bores, which ensured a low distillate pressure drop.

Based on the results of research carried out in Phases I and II, the present Phase III project emphasized scaled-up DCMD studies of much larger rectangular crossflow hollow-fiber membrane modules of type MXFR #3. Since the performance of the process for a given module/flow design depends strongly on the membrane, additional work was initiated at the beginning with small modules of the type used in Phase II. These involved PP hollow fibers of smaller dimensions (280-μm I.D., 397-μm O.D.) and a variety of silicone-fluoropolymer coatings including the case of no coating. Based on the observed DCMD performances of such modules, it was decided to employ larger PP hollow fibers of the 150/330 type (150-μm wall thickness, 330-μm I.D.) and a plasma-polymerized microporous silicone-fluoropolymer coating of the type used successfully in module MXFR #3 of Phase II. The membrane surface area in these modules was varied from 1,970-2,864 square centimeters (cm^2). The internal module dimensions for hot brine flow were 25.4-cm length, 8.57-cm width, and 4.45-cm height. The fibers had mostly a staggered arrangement in 11 or 16 deep layers. Modules having such a design were obtained; the face boxes and face plates were designed to ensure as uniform a hot brine crossflow as possible. The performances of one such large module as well as a stack of two such modules have been investigated with hot brine in DCMD. The experimental investigations carried out involved brine concentrations up to 10%, and brine feed temperature between 40-94 °C. An extended study was also carried out for 5 days. A preliminary cost estimate for DCMD-based desalination of brine has been obtained.

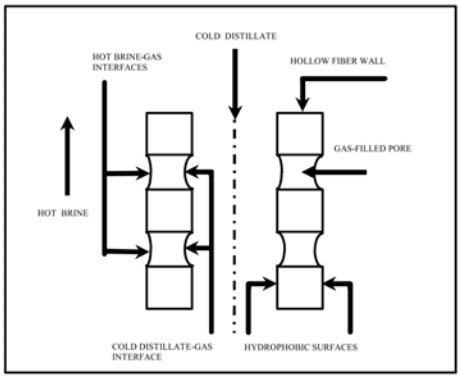

Fig. 1a. Conventional Direct Contact Membrane Distillation

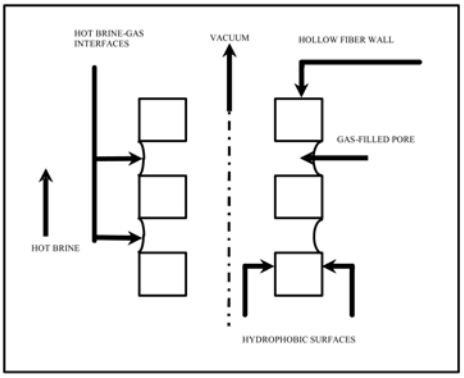

Fig. 1b. Conventional Vacuum Membrane distillation

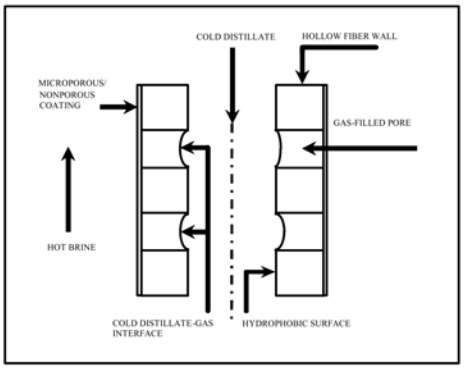

Fig. 1c. Suggested Direct Contact Membrane Distillation

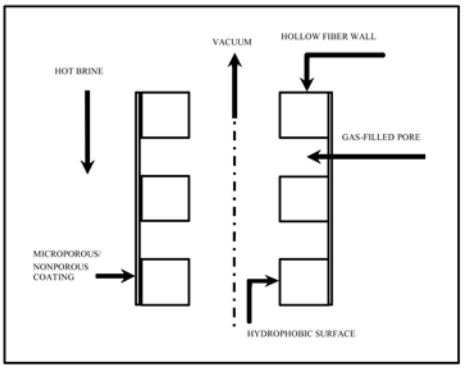

Fig.1d. Suggested Vacuum Membrane Distillation

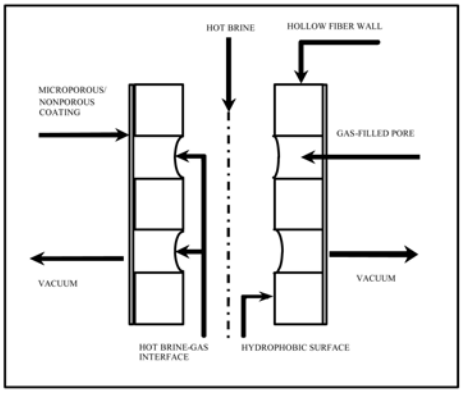

Fig. 1e. Vacuum Membrane Distillation with Hot Brine in Coated Fiber Lumen

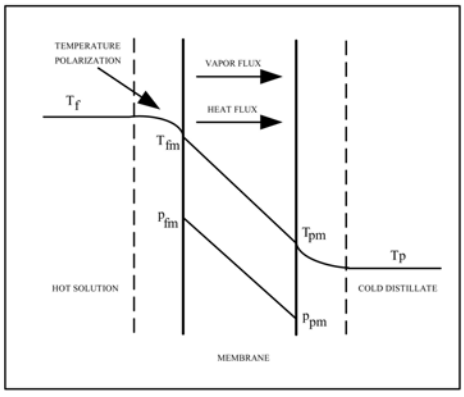

Fig. 1f. Temperature and Partial Pressure Profiles in Direct Contact Membrane Distillation

Figure 1 (a) Conventional Direct Contact Membrane Distillation; (b) Conventional Vacuum Membrane Distillation; (c) Suggested Direct Contact Membrane Distillation; (d) Suggested Vacuum Membrane Distillation; (e) Vacuum Membrane Distillation with Hot Brine in Coated Fiber Lumen; (f) Temperature and Partial Pressure Profiles in Direct Contact Membrane Distillation.

3. Conclusions and Recommendations

1. Two hollow-fiber membrane modules (S/N 1004 and S/N 1005), each having a surface area of 0.2864 square meters (m^2)and a rectangular crossflow of hot brine over the outside fiber diameter have been successfully studied for DCMD-based water recovery from hot feed brine. The brine temperature for module S/N 1004 was varied over a range of 40-94 °C. The membrane surface area in these two modules is more than an order of magnitude larger than those employed in Phase II of this project. The hollow fibers employed in these modules are larger, 330-μm I.D. and 150-μm wall thickness, and correspond to the fibers employed in the most successful module MXFR #3 of Phase II. The microporous plasmapolymerized silicone-fluoropolymer coating on the O.D. of these fibers was somewhat tighter than that in MXFR #3 of Phase II. The fibers are 4 times longer than those in Phase II. Module S/N 1004 has been used for a cumulative time of around 300 hr and continuously over a period of 5 days/127 hrs. We have not encountered any salt leakage into distillate streams.

2. A water vapor flux of 60 $kg/m^2 \cdot h$ based on the fiber I.D. was achieved at 90 °C in DCMD in the module S/N 1004 with the hot brine in rectangular crossflow on the fiber O.D. and cold distillate (at an inlet temperature of 34 °C) in the fiber bore. This water flux value is quite high and demonstrates that the high flux values achieved in Phase II using much smaller modules can also be achieved in much larger modules. The horizontal crossflow based hollow-fiber membrane modules having the appropriate microporous silicone-fluoropolymer coating on the outside surface of larger diameter porous PP fibers appear to be scalable. However, to ensure scalability, attention must be paid to the cold distillate flow rate, which must be sufficient to prevent too high a rise in the distillate outlet temperature. This becomes especially important for larger modules having much longer hollow fibers.

3. Among a number of ways to increase the membrane surface area exposed to a particular hot brine feed stream, stacking a number of identical modules along the flow path is a potential option. Studies in this project using stacked modules S/N 1004 and S/N 1005 have demonstrated that it is indeed a viable option. This allows extraction of the sensible heat via reasonable values of water vapor flux from the hot brine even as its temperature decreases along the flow path.

4. The DCMD process using the membranes of this project can successfully extract water vapor from brine having as much as 10% salt. The water vapor flux is reduced marginally by the increase in salt concentration. Therefore, the DCMD process may be employed to extract water from brine concentrates and aid in their disposal by substantial volume reduction. We foresee no problem handling brines of even higher concentration.

5. This DCMD process and the membrane modules are quite productive even when the hot brine feed temperature is significantly lower than 80-90 °C, which yield high water vapor fluxes. A 60 °C brine feed yielded 20 kg/m^2·h water vapor flux, which is quite reasonable.

6. The 5-day-long continuous DCMD run using module S/N 1004 with no salt leakage at all has demonstrated that this scaled-up module can perform as well as the much smaller module MXFR #3 of Phase II both in terms of water vapor flux and distillate water quality. Fouling was not observed much since a 1-μm microfilter was employed as in most hollow-fiber membrane-based processes. The stable water vapor flux of around 54-58 kg/m^2·h is quite high and is quite attractive. Further it provides considerable support to the assumed value of water flux employed in our economic calculations.

7. There are residual problems in potting of the larger fibers in the larger modules. The possibility of subsequent water leakage through some pores wetted by epoxy during potting has to be eliminated. Applied Membrane Technologies Inc. (AMT) Minnetonka, Minnesota, is aware of this problem and is taking steps to solve it.

8. The results of this project lend support to the idea of a smaller pilot plant study where multi-module stacks may be employed to yield 1-5 gallons per minute (gpm) of distillate.

9. It is useful to replace a multimodule stack with one module which is deeper in the shell-side hot brine flow direction containing many more layers of hollow fibers.

10. The DCMD process should be investigated using hot brine of concentration in the range of 10-40% for potential applications in desalination concentrate volume reduction.

11. Future studies identified in item 10 above may also involve addition of calcium sulfate, calcium carbonate ($CaSO_4$, $CaCO_3$) to the feed brine solution, running the system without any pretreatment followed by cleaning of the scales, as well as running the system with nanofiltration as a pretreatment.

4. Work Performed

4.1 Experimental Details

4.1.1 Membrane Modules

During this period, five small rectangular crossflow hollow-fiber modules (inner dimensions: length - 6.4 cm, width - 2.5 cm, height - 1.8 cm) and four much larger rectangular crossflow hollow-fiber modules (inner dimensions: length - 25.4 cm, width - 8.57cm, height - 4.45cm) were designed by us for direct contact membrane distillation. These modules with open faces were received from AMT.

Each of the five small rectangular modules contained 456 fibers (PP 50/280) (280-μm I.D., 50-μm wall thickness) manufactured by Membrana, Wuppertal, Germany. The porous fibers in modules MXFR #11, MXFR #12, and MXFR #13 were plasma-coated by AMT with silicone-fluoropolymer having different thicknesses and pore mouth openings; the fibers in MXFR #14 were coated only with Teflon; the fibers in MXFR #15 were uncoated. This variety in fiber coating was needed to facilitate selection of the appropriate fiber coating and fiber type in Task 1 described in section 4.1.2. The details of these five modules are shown in table 1a.

Table 1a. Details of the Small Membrane Modules and Hollow Fibers

Particulars	MXFR #11	MXFR #12	MXFR #13	MXFR #14	MXFR #15
Support membrane type	PP 50/280 Accurel Membrana				
Support membrane	PP				
Fiber O.D., μm	397				
Fiber I.D., μm	280				
Wall thickness, μm	50				
Maximum pore size, μm	~ 0.2				
Membrane porosity, %	Unknown				
Coating	Silicone fluoropolymer[1]			Teflon	None
Arrangement of fibers	Staggered				
No. of fibers	12×38= 456				
Effective fiber length, cm	6.4				
[2]Effective membrane surface area, cm^2	256.6				
[3]Effective cross-sectional area for shell side liquid flow, cm^2	6.34				
Module frame (internal dimensions)	Length: 6.4 cm, width: 2.5 cm, height: 1.8 cm				
Packing fraction	0.13				
Shell-side flow mode	Crossflow				
Fabricated at	AMT, Minnetonka, Minnesota				

[1] The coating of the MXFR #11 is similar to the MXFR #9 (Phase II Project). The MXFR #12 has a thinner coating of the same composition as the MXFR #11. The MXFR #13 has less silicone in the coating than the MXFR #11.

[2] Based on fiber internal diameter.

[3] Based on open area for flow = frame cross sectional area (6.4 × 2.5 cm^2) – fiber projected area (number of fibers in one layer × fiber O.D. × length of fiber cm^2).

All porous hollow-fiber membranes in the four larger modules had a plasmapolymerized silicone-fluoropolymer coating on the outer surface having a microporous structure similar to MXFR #3 used in Phase II Project (Sirkar and Li, 2003). The precursor of the coated membrane in these larger modules is the PP 150/330 hollow fiber (330-μm I.D., 150-μm wall thickness) manufactured by Membrana. All fibers in the modules were staggered in arrangement. The only difference between these four larger modules is that there are 748 hollow fibers in modules S/N 1002 and S/N 1003, and 1,088 fibers in modules S/N 1004 and S/N 1005. The design of crossflow rectangular modules allows achievement of a much higher brine-side heat transfer coefficient (shell side) compared to that achieved in parallel flow at similar Reynolds numbers (per the conclusions in the Phase II Project). The ultrathin coating has high water vapor permeance and potentially makes the fiber permanently nonwettable from the shell side under the operating conditions. Compared to the coated PP 50/200 and PP 50/280 fibers, these coated PP 150/330 hollow fibers have a much smaller membrane heat transfer coefficient[1] (660 watts per square meter Kelvin [W/m^2K]), which can effectively reduce the conductive heat loss. The large diameters of the hollow fibers allow us to get relatively high brine-side Reynolds number, which raises the overall boundary layer heat transfer coefficient and reduces the polarization coefficients of temperature and concentration. On the other hand, the larger bore hollow fibers allows the cold distillate flow rate to be high so that we can maintain a high ΔT vis-à-vis the hot brine at a low value of lumen pressure drop. The characteristics of the larger membrane modules and their membranes are given in table 1b.

Figure 2a shows the photograph of a smaller rectangular crossflow module. Figure 2b is a photograph of a larger rectangular crossflow module along with that of a smaller one. A photograph of the fiber arrangement in a module is shown in figure 2c.

Since the modules received from AMT were only rectangular channels having coated hollow fibers running across and two open faces, we designed and fabricated a diverging section and a converging section to allow the liquid to flow uniformly in cross flow outside of and perpendicular to the fibers. The diverging section and the converging section were two boxes having a curved shape (figure 3). Two face plates were made from two flat plastic sheets. On each sheet, 104 smaller holes having a wide size distribution were opened (the hole sizes were such that the holes at the center were smaller, while those further away were progressively larger) (figure 4). The design mentioned above ensured that the feed solution flowed uniformly through the shell side of the fibers. The

[1] The values of membrane heat transfer coefficient were calculated based on the experimental data in Phase II Project. The definition of heat transfer coefficient and the correlations will be illustrated in Section 4.1.2, "Experimental Apparatus and Procedures."

Table 1b. Details of the Larger Membrane Modules and the Hollow Fibers

Particulars	S/N 1002	S/N 1003	S/N 1004	S/N 1005
Support membrane type	PP 150/330 Accurel Membrana			
Support membrane	PP			
Fiber O.D., μm	630			
Fiber I.D., μm	330			
Wall thickness, μm	150			
Maximum pore size, μm	>0.2 up to 0.6			
Membrane porosity	~0.6-0.8			
Coating	[1]Silicone fluoropolymer			
Arrangement of fibers	Staggered			
No. of fibers	11×68=748		16×68=1088	
Effective fiber length, cm	25.4			
[2]Effective membrane surface area, cm^2	1970		2864	
[3]Effective cross-sectional area for shell side liquid flow, cm^2	108.86			
[4]Cross-sectional area for tube side liquid flow, cm^2	0.63		0.93	
Rectangular module frame (internal dimensions)	L: 25.4 cm, W: (3.25+3.5) ×2.54/2 = 8.57cm, H: 4.45 cm			
Packing fraction of fibers	0.227	0.227	0.22	0.22
Shell side flow mode	Crossflow			
Fabricated at	AMT, Minnetonka, Minnesota			

[1] All membranes represent a recipe similar to the copolymer coating on MXFR #3 of Phase II Project. Coating developed by Applied Membrane Technology, Inc., Minnetonka, Minnesota.

[2] Based on fiber internal diameter.

[3] Based on open area for flow = frame cross sectional area ($25.4 \times 8.57 cm^2$) – fiber projected area (no. of fibers in one layer × fiber O.D. × length of fiber cm^2).

[4] Lumen side flow cross-section area = fiber number × $(ID/2)^2 \times \pi$.

material used for the face boxes and face plates was translucent polypropylene having a reasonable thickness and thermal resistance.

Two face boxes and face plates were assembled with a rectangular membrane module channel and 10 bolts to constitute the complete device (figure 5). Neoprene gaskets (1/8-inch) were used between the face box, the face plate, and the module channel on each side to seal the parts together. Hot brine was allowed to enter one face box, and then leave the box through the face plate holes, which distributed the liquid flow evenly, and then enter the flow channel. On the other side, the liquid left the channel through the face plate holes and collected in the face box and then flowed beyond the box and thus the module. In this design, between the face plate and the frame containing the fibers, there was space due to the gasket. Further there was a small axial gap around ¼-inch between the module frame surface and the beginning of the fibers. This allowed evening out of any irregularity in the flow out of the face plate into the fibers. The liquid flow was expected to cross the fiber layer uniformly and perpendicularly to ensure good heat and mass transfer. For the five small modules, the face boxes and face plates were the same as those used in the Phase II Project.

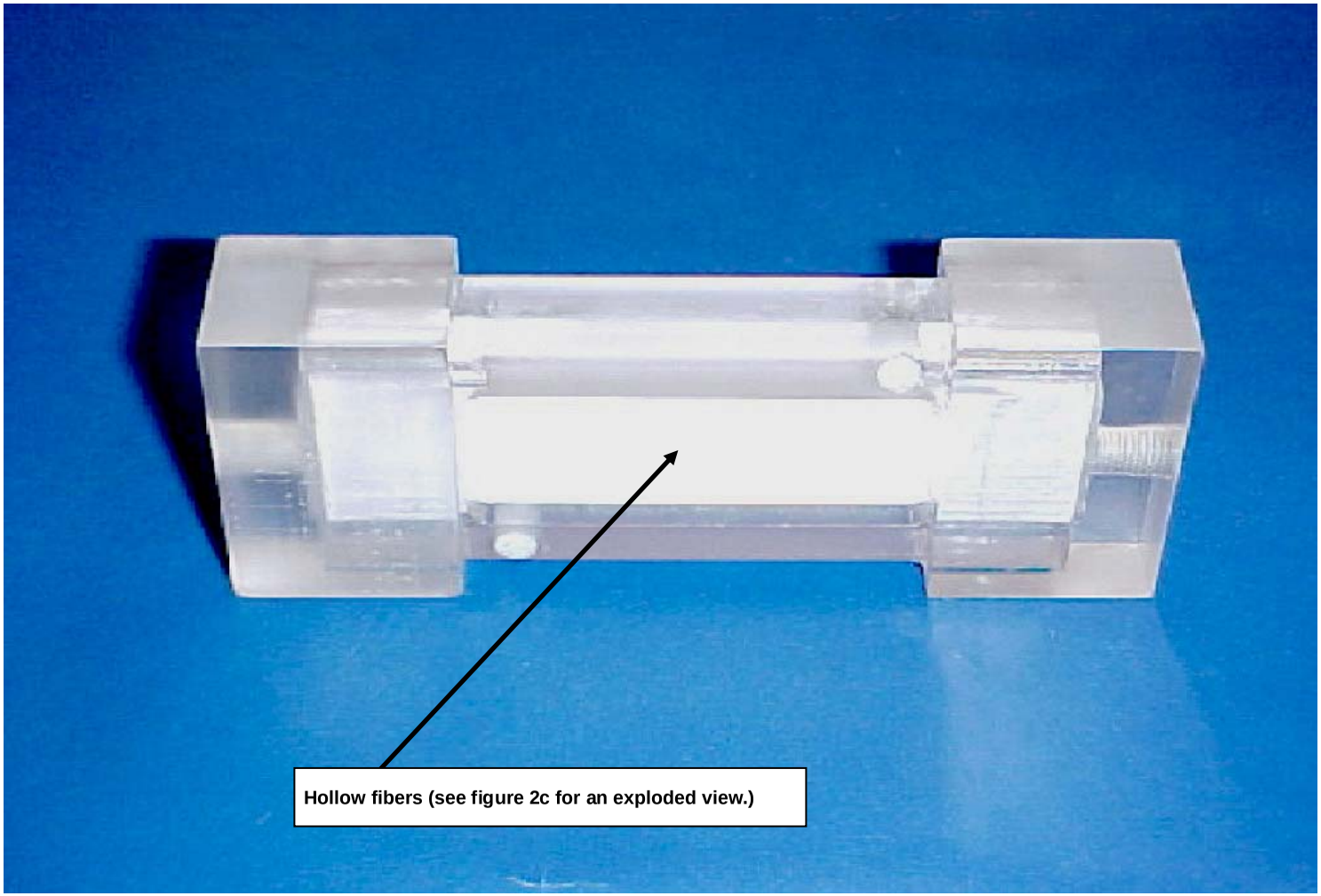

Figure 2a. A smaller rectangular crossflow test module without face plates.

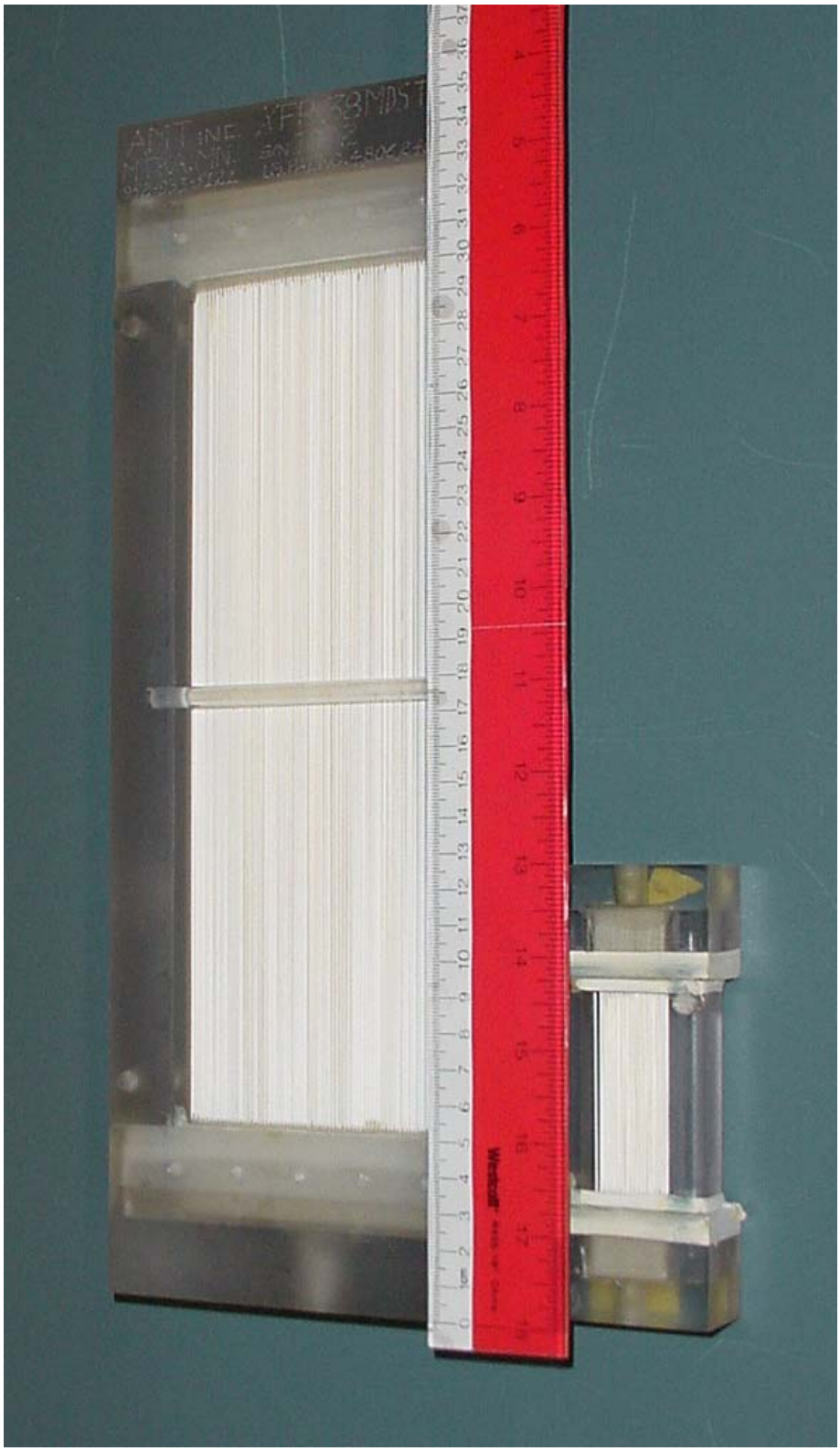

Figure 2b. Photograph of small-size membrane module and larger size module used in Phase III with a scale in between.

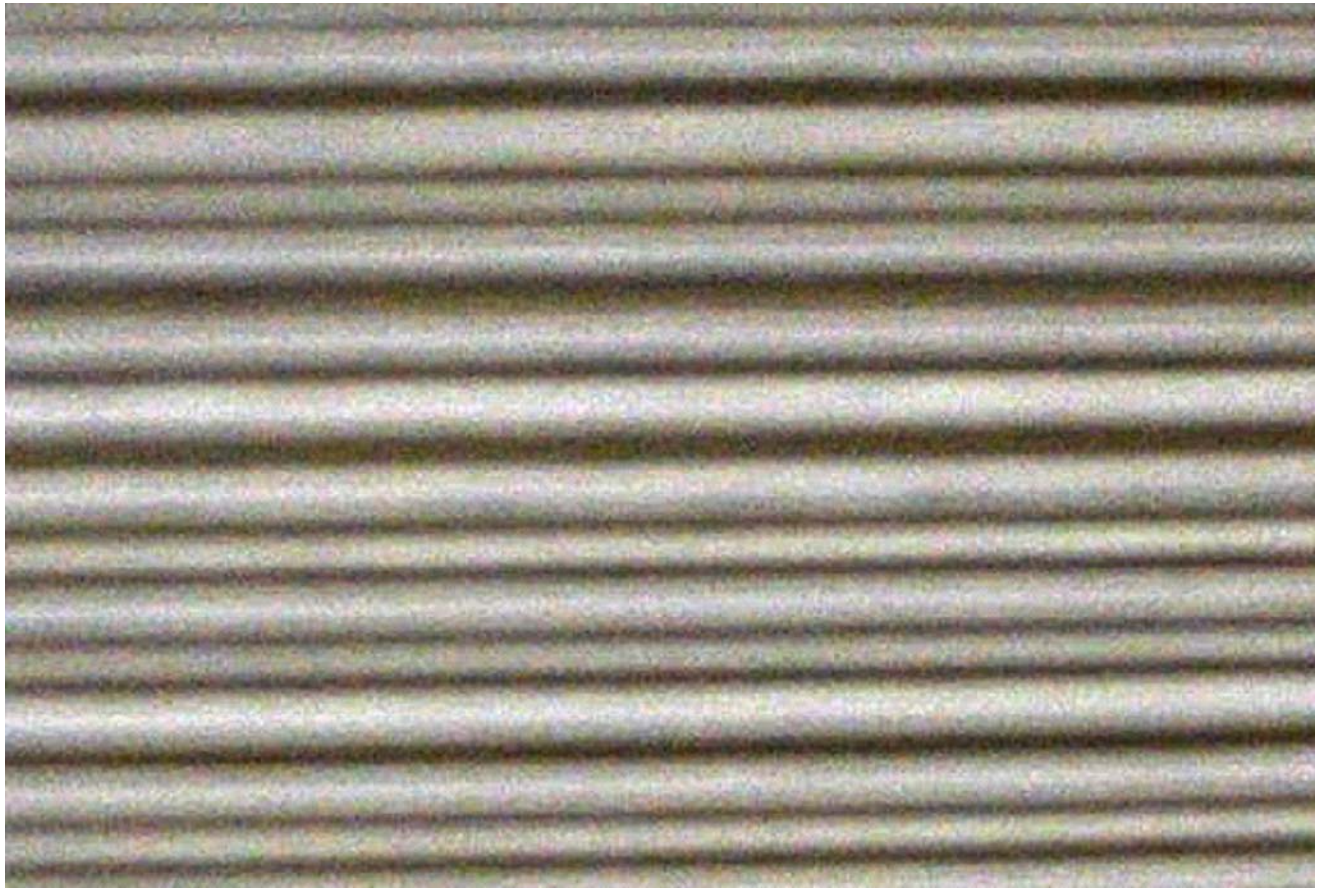

Figure 2c. Arrangement of the coated microporous hollow fibers in a rectangular crossflow text.

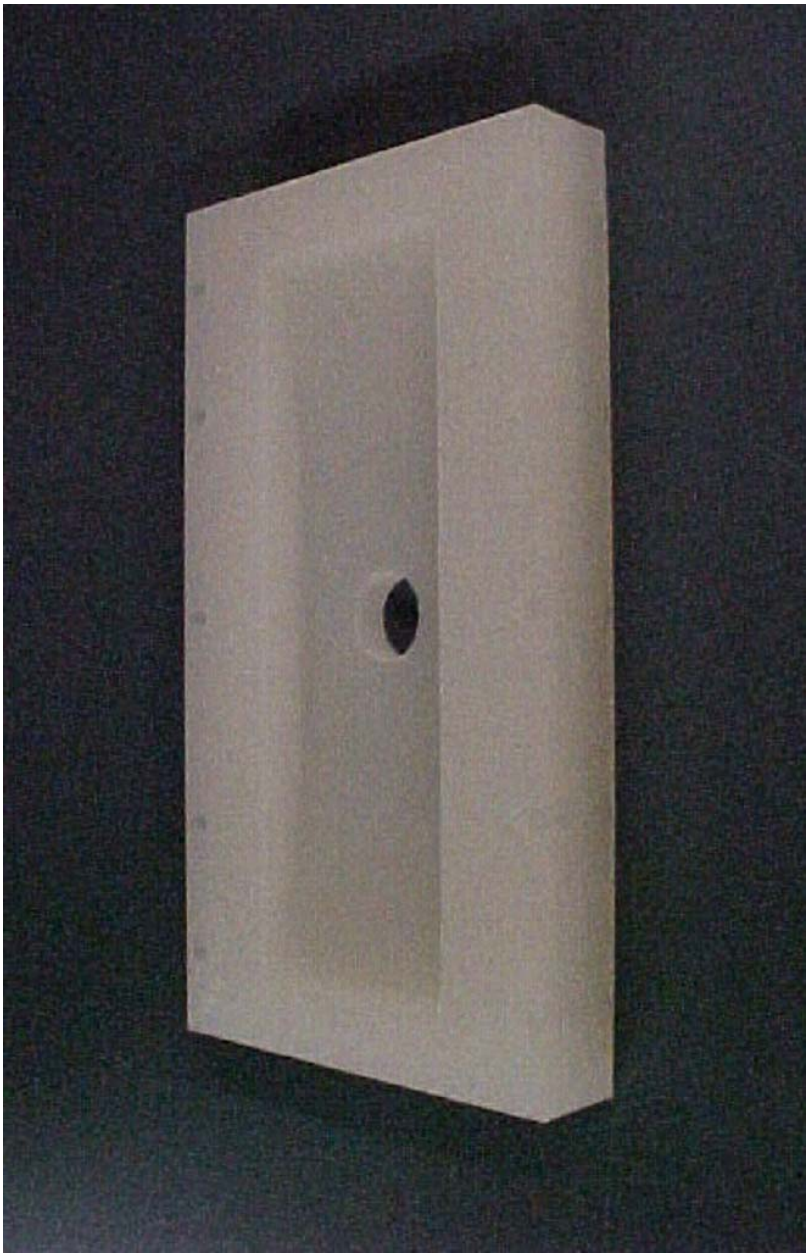

Figure 3. Face fabricated for rectangular crossflow module.

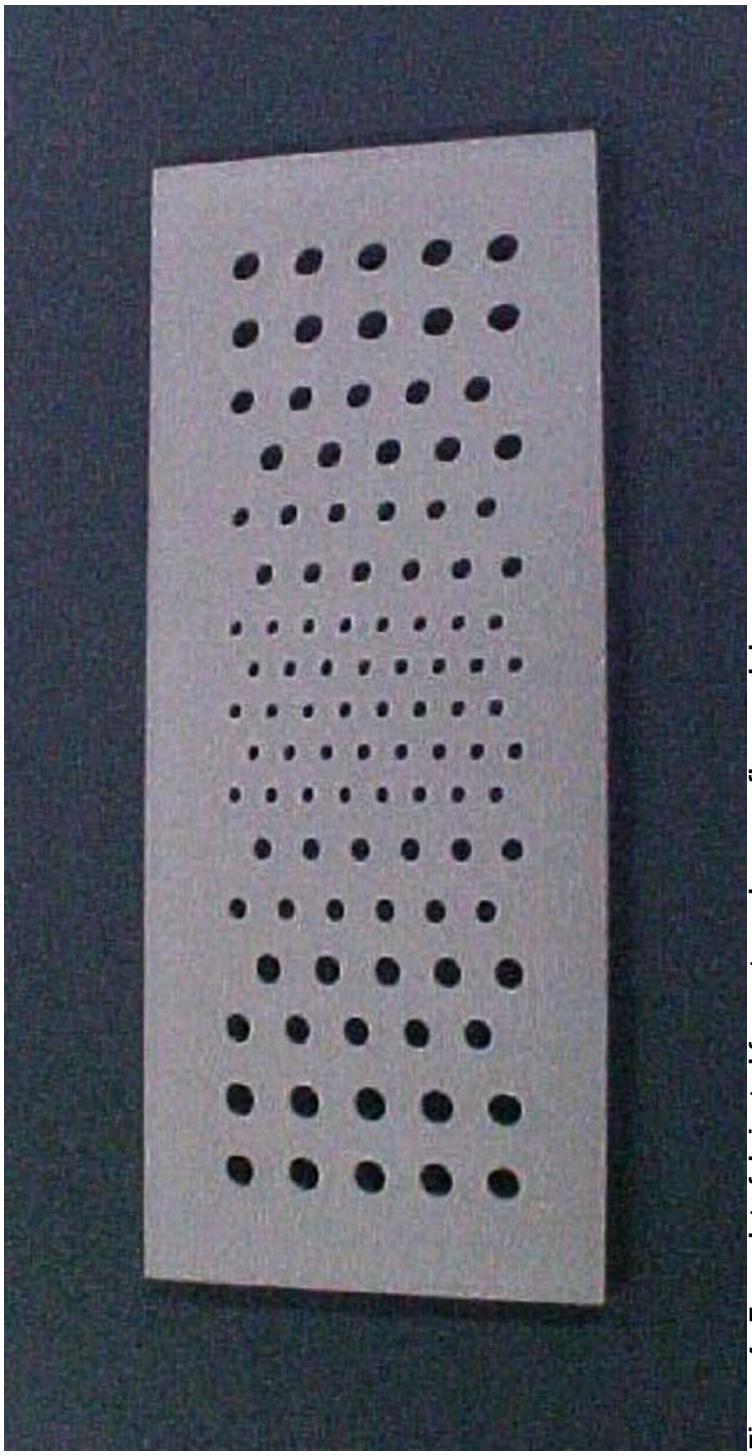

Figure 4. Face plate fabricated for rectangular crossflow module.

Figure 5. Rectangular crossflow test module with face boxes, plates, and assembly.

4.1.2 Experimental Apparatus and Procedures

The experimental apparatus developed could be used to study the DCMD process on a larger scale (compared to that in Phase II). A schematic of the apparatus in terms of a process flow diagram is shown in figure 6a. Figure 6b is a schematic of the electrical connections for the DCMD experimental setup. All of the system piping and storage tanks were thoroughly insulated to minimize heat loss to the environment. Figure 7 shows a photograph of the membrane module assembled in the DCMD system. Figure 8 provides a photograph of the experimental setup of figure 6a. This setup was prepared under Tasks 2 and 3. A summary of the project tasks is provided to provide a perspective.

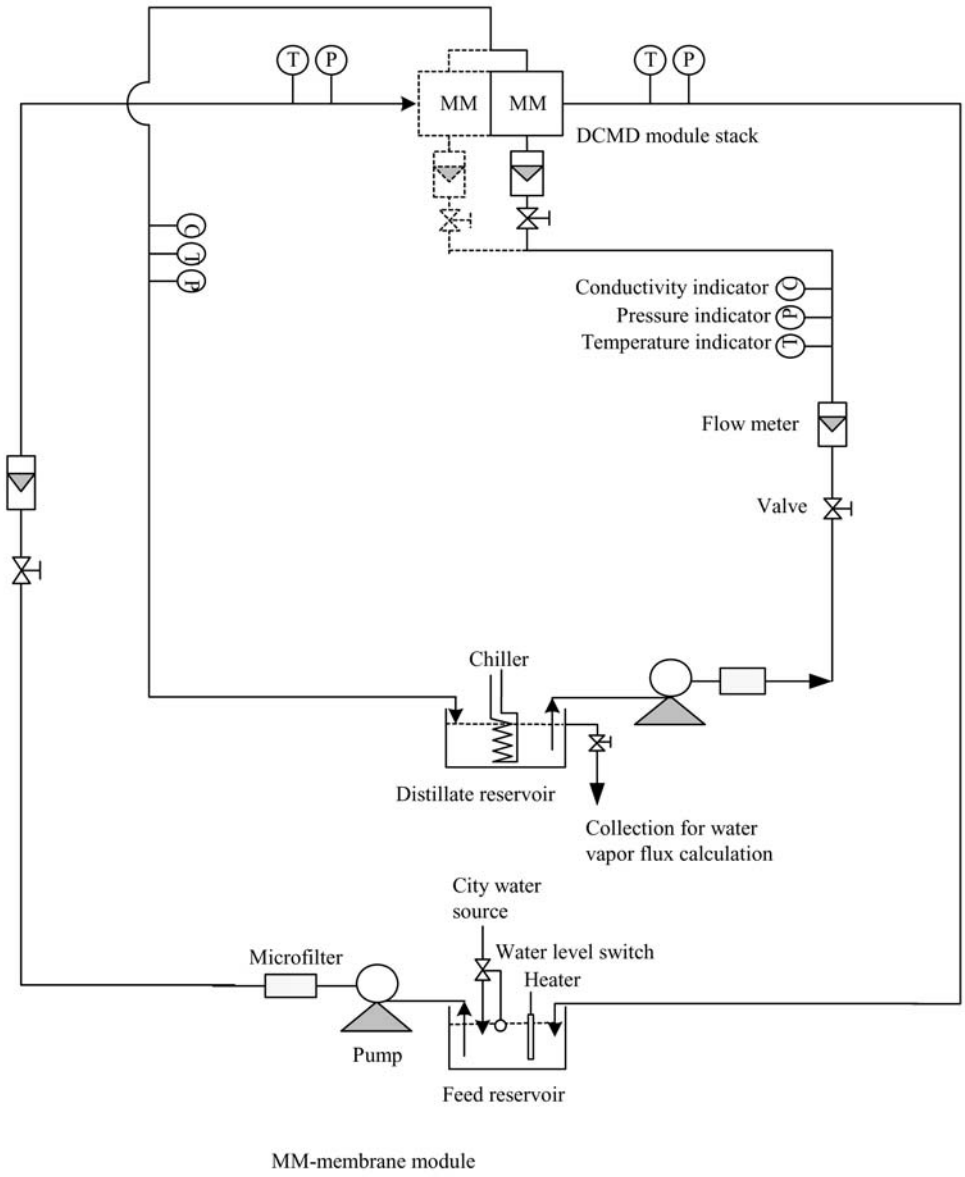

Figure 6a. Process flow diagram for DCMD.

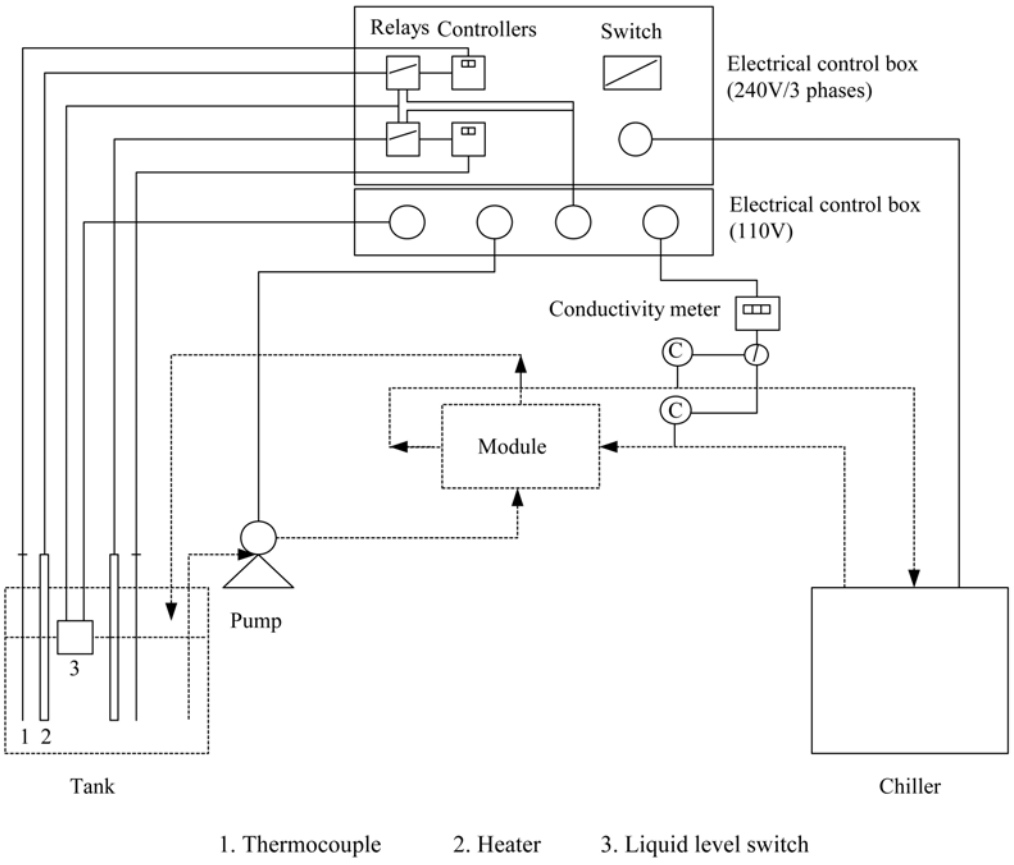

Figure 6b. Schematic of electrical connections for DCMD experimental setup.

Figure 7. Photograph of the membrane module assembled in DCMD system.

Figure 8. Photograph of the experimental setup up figure 6a.

Task 1. Develop large-scale rectangular crossflow hollow-fiber membrane modules having an appropriate coating on the fibers and corresponding DCMD setup.

Task 2. Study the DCMD performances of different membrane modules obtained in Task 1.

Task 3. Study the DCMD performances of a 2-module stack.

Task 4. Develop correlations to facilitate performance prediction of larger systems.

Task 5. Develop a preliminary cost estimate for DCMD-based desalination of brine.

Task 6. Seek information about potential pilot plant studies in the future.

Task 7. Prepare and submit data and reports at appropriate intervals.

DCMD: In the experimental setup for DCMD operation shown in figure 6, city water or brine was introduced to the shell side from a reservoir by a centrifugal pump (model: TE-4-MD-HC, Little Giant Co., Oklahoma City, OK) at a constant flow rate controlled by a ball valve. The flow rate of the liquid system could be varied between 5-40 liters per minute (L/min). Feed solution in a 200-liter stainless steel tank was heated by a heating system having two heaters (OMEGA, EMT-312E2/240 3-phase moisture resistant heater (12 kilowatt [kW]); EMT-309E2/240 3-phase moisture resistant heater (9 kW); total 21 kW of heating capacity), two OMEGA rugged transition joint probes, two OMEGA three-phase DIN rail-mount, solid-state relays, and two OMEGA CN77333 controllers. The temperature controllers maintained the bath temperature at a given value and, thus, maintained a constant entrance temperature for the hot brine/water feed.

Outside the membrane module, the exiting feed was circulated back to the feed reservoir and was re-warmed. For safety, a liquid level switch was installed in the feed tank.

The cooling system was mainly composed of a Remcor chiller having a cooling capacity of 12 kW (model: CH3002A, voltage (full-load amps): 230/60/3, IMI Cornelius Inc., Anoka, Minnesota) with a recirculation pump and a 10-gallon tank. Deionized (DI) water was introduced as the cooling liquid on the fiber lumen side of the module from the reservoir at a constant flow rate. The exiting hot distillate from the module was cooled to a given temperature by the chiller before entering the module again.

Each liquid solution (including feed solution and cooling water) was filtered by passing through a 20-inch postfilter cartridge (1 μm) (model: DGD-2501-20, USFilter-Plymouth Products, Sheboygan, WI) before entering the membrane module.

The inlet and outlet temperatures and pressures of the hot feed and the cold distillate were measured by thermocouples and pressure gauges. The electrical conductivities or the salt concentrations of the distillate into and out of the module were monitored by a conductivity meter (model: CON200 Series, Oakton Instruments, Vernon Hills, IL).

When the readings of the flow rates of the hot solution, cold distillate water, and the four inlet and outlet temperatures reached constant values, it was assumed that the experimental conditions had reached a steady state; then the distillate spilled from the cooling water reservoir beyond a certain level was collected. The volume of the distillate collected in a certain time was used to calculate the water vapor flux through the membrane under the given experimental conditions. Water vapor flux was calculated from the following relation:

$$\text{Water vapor flux } \left(\frac{\text{kg}}{\text{m}^2\text{ - h}}\right) = \frac{\text{vol. of water transferred (l)} \times \text{density of water (kg/l)}}{\text{membrane area (m}^2\text{)} \times \text{time (h)}} \quad (1)$$

Here, the membrane area was calculated based on the hollow fiber inside area, $s = n\pi d_i L$, where n is the number of fibers in a membrane module; d_i is the fiber inside diameter (I.D.); L is the fiber length.

Leak Testing: All membrane modules, listed in tables 1a and 1b, were tested for leakage before DCMD measurements. Before the leak tests, each membrane module was activated by circulating DI water in the shell side and tube side at a very low flow rate and at room temperature for at least 10 hrs. Then the module was assembled in the DCMD system. A solution of 1% NaCl at 85 °C flowed through shell side at a constant flow rate of 0.4-2 L/MIN for small modules and 5-25 L/min for larger modules (the pressure drop was kept in the range of 1-2.5 pounds per square inch [psi]), and DI water flowed through the tube side at a low flow rate at room temperature. The conductivity of the distillate was monitored with increasing brine flow rate. If the conductivity of the distillate water rose evidently with operating time, the test membrane module was leaking. Otherwise, the test membrane module was leak free. Besides, filling DI water in the tube side and keeping a constant pressure for a long time is another way to check the leakage status of a hollow-fiber module.

All four modules were found to be leaking at 3 psi of water on the lumen side. The extent of leakage in modules S/N 1004 and S/N 1005 was slight; however, there was considerable leakage in modules S/N 1002 and S/N 1003. The leakage of the modules S/N 1004 and S/N 1005 was solved by gluing with epoxy in our lab for DCMD measurements. Modules S/N 1002 and S/N 1003 have been sent back to AMT for further treatment. It was found that the leakage was mainly from the fibers near the two ends of the modules; it was possibly developed during fabrication of these modular channels. This suggests that the distillate pressure in the lumen side should be lower than 3 psi. Otherwise, the distillate water will penetrate through the membrane wall from the lumen side to the shell side resulting in loss of some distillate as opposed to contamination of the distillate by the brine. That means that the water vapor flux would be affected negatively to some extent by the loss of permeation area and by the lower velocity of operation on the lumen side.

Gas Permeation: A system was also established for the measurement of gas permeance of the coated porous hollow-fiber membranes using a gas permeation apparatus (figure 9). The N_2 gas from the cylinder permeated through the membrane from the tube side to the shell side. The pressures of upstream and downstream were measured by Ashcroft Test Gauge (PT. No. 63-5631). The downstream flow rate of the gas was measured using a soap bubble flow meter. During the permeation measurements, the upstream pressure was maintained at a constant pressure, between 0.1-0.6 pounds per square inch gage (psig) (0.5-3.1 cm mercury [Hg] gage). The permeation measurements were made at room temperature. The permeant gas was nitrogen (N_2).

The N_2 permeance of the hollow-fiber membranes was related to the measured steady-state permeation rate of nitrogen through the membrane by equation (2):

$$\frac{Q_{N_2}}{\delta_M}(permeance) = \frac{P_1 V_1 T_0}{P_0 T_1 \cdot s \cdot \Delta P_{N_2}} \qquad (2)$$

In equation (2), T_0 = 273.15 K, P_0 = 760 Torr, ΔP_{N_2} corrected to standard temperature and pressure (STP) is the pressure difference across the membrane, s is the inside membrane area, P_1 is the atmospheric pressure, T_1 is the room temperature, V_1 is the volume flow rate of gas through the membrane during measurement at room temperature, Q_{N_2} is the permeability coefficient of N_2 permeation through the membrane of effective thickness δ_M .

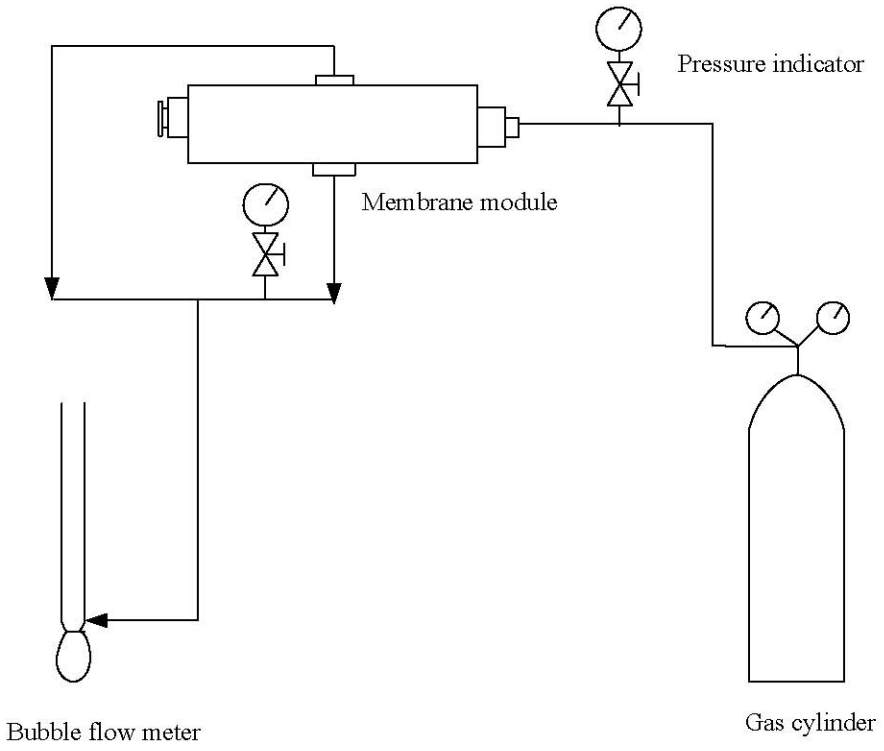

Figure 9. Experimental setup for membrane gas measurement.

Calculation of Reynolds numbers: Reynolds number is normally defined in the following way:

$$\mathrm{Re} = \frac{D \times V \times \rho}{\mu} \tag{3}$$

Where:

Re: Reynolds number; D: characteristic dimension; V: velocity; ρ: density; μ: dynamic viscosity (absolute viscosity).

In Tasks 2, 3, and 4 of this project, the Reynolds numbers of the hot feed or the cold distillate flowing through the shell or the tube side were defined as diameter–based Reynolds number (Re_d). In the calculation of Re_d based on equation (3), fiber I.D. (d_i) and linear velocity are used for tube-side parallel flow, and fiber O.D. and interstitial velocity for shell-side crossflow.

Interstitial velocity (V_I) = brine flow rate/open area for flow through the shell side (4)

The open area for flow through the shell side has been defined at the bottom of tables 1a and 1b.

Linear velocity (V_L) = flow rate/open area for flow through the tube side (5)

In the MD literature, boundary layer heat transfer coefficients are almost always estimated from empirical correlations. For laminar flow in a circular tube (i.e., fiber lumen), Sieder-Tate equation is popularly employed (Gryta et al., 1997; Hobler, 1986):

$$Nu = 1.86(d_i \,\mathrm{Re}_d \,\mathrm{Pr}/L)^{0.33}(\mu/\mu_w)^{0.14} \tag{6}$$

where Nusselt number, $Nu = h_p d_i / k$, $\mathrm{Re}_d = V_L d_i \rho / \mu$, and the Prandtl number, $\mathrm{Pr} = c_p \mu / k$. Further h_p is the tube-side boundary layer heat transfer coefficient, d_i is the tube/fiber I.D., k is the liquid thermal conductivity, V_L represents the linear velocity of liquid flowing on the tube side, μ_W is the liquid viscosity evaluated at the tube-wall temperature, c_p is the liquid heat capacity, and L is the tube length. The viscosity correction factor $(\mu/\mu_w)^{0.14}$ normally is negligible for MD applications (Lawson and Lloyd, 1996b). Equation (6) is suitable for laminar tubular flow conditions (Re_d <2,100).

For the calculation of the boundary layer heat transfer coefficient of liquid flowing on the shell side of rectangular crossflow hollow-fiber modules, we have not been able to locate any publication relative to this subject. *Zukauskas equation* is often used in the calculation of the Nusselt number for crossflow over tube bundles in heat exchangers when $10 < \mathrm{Re}_d < 5\times10^2$ (Incropear and Dewitt, 2002; Kreith and Bohn, 2001):

$$Nu = 1.04\,\mathrm{Re}_d^{0.4}\,\mathrm{Pr}^{0.36}(\mathrm{Pr}/\mathrm{Pr}_w)^{0.25}F_c \tag{7}$$

where Nusselt number, $Nu = h_f d_o / k$. Further h_f is the shell-side boundary layer heat transfer coefficient, d_o represents the tube/fiber O.D., Pr_w is the Prandtl number evaluated at the tube-wall temperature, F_c is the tube-row correction factor. All properties except Pr_w are evaluated at arithmetic mean of the fluid inlet and outlet temperatures. We report these equations here to provide a basis for using Re_d in reporting our data even though there is a problem due to fibers potentially moving and any irregularity of flow from the entrance section. Further the velocity used in Re_d is the interstitial velocity (V_I) which takes into account the fiber packing density.

Definitions of Heat Transfer Coefficients: At steady state, the effective heat flux at the two liquid-membrane interfaces (figure 1f) may be described by

$$Q = h_f A_{rf} (T_f - T_{fm}) = h_f A_{rf} \Delta T_F = h_p A_{rp} (T_{pm} - T_p) = h_p A_{rp} \Delta T_P \quad (8)$$

where Q is the effective heat flux through the membrane, ΔT_F is the temperature difference between brine bulk temperature, T_f and the temperature of the brine-membrane interface on the feed side, T_{fm}, ΔT_P is the temperature difference between the temperature of the membrane-distillate interface, T_{pm}, and the distillate bulk temperature on distillate side, T_p. In the hollow-fiber module, the membrane thickness is comparable with the inside diameter of the fiber. This results in considerable difference between the outside and inside area of the hollow-fiber membrane. In this case, a change of the membrane surface area for heat transfer should be taken into account. Here, A_r is the area ratio for the heat transferred through the membrane. Since we have selected the internal diameter-based surface area as our basis, therefore A_{rf} for the interfacial area between the hot brine and the O.D. is (d_o / d_i); the corresponding A_{rp} is (d_i / d_i)=1 .

At the pore mouth on the membrane surface, water from the brine is vaporized; the heat flux transferred by this vapor flux across the membrane is

$$Q_V = h_v A_{r\ln} (T_{fm} - T_{pm}) = h_v A_{r\ln} \Delta T_m = N_V A_{r\ln} \Delta H_V \quad (9)$$

where h_v is the heat transfer coefficient related to the water vapor flux, ΔT_m is the trans-membrane temperature difference $(T_{fm} - T_{pm})$, N_V is the mass flux of water vapor across the membrane, and ΔH_V is the heat of vaporization/mass of water. The surface area ratio ($A_{r\ln}$) is defined as ($d_{r\ln} / d_i$) where $d_{r\ln}$ is the logarithmic mean diameter, (($d_o - d_i$) / ln(d_o / d_i))).

Heat is additionally conducted through the nonporous solid polymeric part of the membrane and the gas phase that fills the pores at a rate

$$Q_m = h_m A_{r\ln} (T_{fm} - T_{pm}) = h_m A_{r\ln} \Delta T_m \quad (10)$$

where h_m is the membrane heat transfer coefficient. Further

$$h_m = \varepsilon h_{mg} + (1 - \varepsilon) h_{ms} \quad (11)$$

where ε is the membrane porosity, and h_{mg} and h_{ms} represent the heat transfer coefficients of the vapor/gas within the membrane pores and the solid polymeric membrane material respectively. The coefficient h_{mg} is generally an order of magnitude smaller than h_{ms}; for example, the thermal conductivities of polypropylene, air and water vapor are respectively, k_{PP} = 0.17 watts per meter Kelvin [W/m·K], k_{air} = 0.03 W/m·K and $k_{waterwapor}$ = 0.025 W/m·K in the temperature range from 20-100 ^{o}C. Therefore, the value of h_m is minimized by maximizing the membrane porosity; DCMD process prefers high porosity and

high wall thickness membranes so that conductive heat loss through the membrane can be reduced considerably. The plasmapolymerized microporous coating introduces a complication which may be considered an unknown at this time for modeling purposes.

The total effective heat flux across the membrane, Q, is related to Q_V and Q_m by

$$Q = Q_V + Q_m = (h_v + h_m) A_{r\ln} \Delta T_m \tag{12}$$

Since the heat transfer mechanism in DCMD is described as a series of resistances, the overall heat transfer coefficient of the DCMD process, U, is conventionally obtained as a series of resistances defined here with respect to A_{rp}: brine film resistance ($1/h_f$), effective membrane resistance ($1/h_c$) and distillate film resistance ($1/h_p$):

$$UA_{rp} = \left[\frac{1}{A_{rf} h_f} + \frac{1}{A_{r\ln} h_c} + \frac{1}{A_{rp} h_p} \right]^{-1} \tag{13}$$

where

$$h_c = h_m + h_v = h_m + \frac{N_V \Delta H_V}{\Delta T_m} \tag{14}$$

Incorporation of expression (14) in relation (13) leads to the following complex relationship between the overall heat flux Q and the mass flux of water vapor N_V:

$$Q = \left[\frac{1}{A_{rf} h_f} + \frac{1}{A_{r\ln} h_m + N_V A_{r\ln} \Delta H_V / \Delta T_m} + \frac{1}{A_{rp} h_p} \right]^{-1} \Delta T = UA_{rp} \Delta T \tag{15}$$

where ΔT is the bulk temperature difference, $T_f - T_p$; the value of A_r for U depends on the basis of calculation, it can be A_{rf} or A_{rp}, or $A_{r\ln}$. Here we have taken A_{rp} as the basis.

Of the two components of the membrane heat transfer coefficient, h_c, the component h_v is responsible for the most important quantity in DCMD, namely, the water vapor flux. To maximize the latter for a given h_v, ΔT_m should be maximized, which, in turn, will maximize N_V by increasing the temperature T_{fm} which determines the vapor pressure of water at the brine-membrane pore mouth. The value of T_{fm} is usually described via the temperature polarization coefficient (TPC):

$$TPC = \frac{T_{fm} - T_{pm}}{T_f - T_p} = \frac{\Delta T_m}{\Delta T} \tag{16}$$

TPC is the fraction of external applied thermal driving force that contributes to the mass transfer.

If we define an overall boundary layer heat transfer coefficient h via

$$\frac{1}{hA_{r\ln}} = \frac{1}{A_{rf}h_f} + \frac{1}{A_{rp}h_p} \tag{17}$$

then TPC can be defined by

$$TPC = \frac{\Delta T_m}{\Delta T} = 1 - \frac{UA_{rp}}{hA_{r\ln}} \tag{18}$$

Temperature polarization has a negative influence on the productivity of the membrane distillation process as a consequence of the decrease in the temperature of the brine (therefore, the water vapor pressure) on the evaporation surface and its increase on the condensation surface. Ideally, TPC should equal 1, but usually it is lower.

Mass Transfer in DCMD: Mass transfer in hollow-fiber modules usually is described via an overall mass transfer coefficient, which is the reciprocal of an overall mass transfer resistance. This overall mass transfer resistance is the sum of the individual resistances of three regions: the tube-side boundary layer in the fiber, across the membrane, and the boundary layer outside the fibers. Each individual resistance is in turn proportional to the reciprocal of an individual mass transfer coefficient. If one of the three individual coefficients is much smaller than the other two, it can dominate the overall mass transfer coefficient. The overall mass transfer coefficient in DCMD is described by:

$$\frac{1}{A_{rp}K} = \frac{1}{A_{rf}k_f} + \frac{1}{A_{r\ln}Hk_m} + \frac{1}{A_{rp}k_p} \tag{19}$$

where K is the overall mass transfer coefficient, k_f, k_m, and k_p are the individual mass transfer coefficients for the hot brine feed, the membrane, and the cold distillate. H is the Henry's Law constant for water, the equilibrium concentration in gas divided by that in the liquid.

Resistance to mass transfer through the membrane comes from the presence of air trapped in the porous membrane structure, i.e., pore size, porosity, and tortuosity. The resistance to the flow of vapor through the porous membrane can be

described by Knudsen diffusion or Poiseuille flow or a combination of both. The equations developed to describe the vapor transfer in membrane pores suggest equation (19) as an overall, basic equation.

Schofield et al. (1987) and Pena et al. (Godino et al., 1996; Pena et al., 1998) found that the membrane mass transfer coefficient, k_m, is slightly temperature dependent, decreasing 3% with a 10 °C increase in the mean temperature. This suggests that for water flux through 0.2 to 1.0 μm pores, Knudsen flow is dominant. The membrane mass transfer coefficient can also be affected by pressure, but for most cases the membrane mass transfer coefficient is mainly constant (Schofield et al., 1990c; Martinez-Diez and Vazquez-Gonzalez, 1996). If convective transport is dominant, k_m will be strongly dependent on the membrane pore geometry. If diffusive transport is dominant, the controlling parameter will be the average mole fraction of air present within the pores. In this case, the microporous coating on the surface will introduce an additional complexity to this picture. However, in most cases, the relationship of the mass water vapor flux and the membrane mass transfer coefficient can be described as

$$N_V = k_m A_{rp} (p_{fm} - p_{pm}) = k_m A_{rp} \Delta p_m \tag{20}$$

In MD, most of the selectivity or separation is attributed to vapor–liquid equilibrium at the liquid boundary layers. From the Antoine equation (Schofield et al., 1987) the water vapor pressure (and therefore the DCMD driving force Δp_m) could be estimated:

$$p^o_{water} = \exp\left[23.238 - \frac{3481}{T - 45}\right] \tag{21a}$$

where p^o_{water} is expressed in units of Pa, and T is in K.

$$\Delta p_m = \exp\left[23.238 - \frac{3481}{(T_{fm} + 273) - 45}\right] - \exp\left[23.238 - \frac{3481}{(T_{pm} + 273) - 45}\right] \tag{21b}$$

The total pressure, P, within the membrane may be greater than the saturation pressure due to the partial pressure exerted by dissolved air. As a rule of thumb, the total pressure within the membrane is usually equivalent to the static pressure above the liquids in the feed and permeate holding tanks. For non-ideal binary mixtures, the partial pressures can be determined from

$$p_i = y_i P = x_i a_i p_i^0 \tag{22}$$

where y_i and x_i are the vapor and liquid mole fractions of i respectively, p_i^0 is the saturation pressure of pure i, and a_i is the activity coefficient of i in the

solution. The value of a_i can either be calculated from one of a variety of available equations or it can be estimated for available experimental data. An equation based on published experimental data to determine the activity of water in NaCl solutions is presented as (Lawson et al., 1997)

$$a_{water} = 1 - 0.5x_{NaCl} - 10x_{NaCl}^2 \tag{23}$$

where x_{NaCl} is the mole fraction of NaCl in water solution.

For MD performances with pure water or dilute water solution, the boundary layer resistances to mass transfer generally can be ignored. However, in a MD separation process with a concentrated solution as feed, mass transfer across boundary layers or concentration polarization can play a significant role in the performance of an MD system. The boundary layers can increase the overall resistance to mass transfer, and they can cause undesirable solute concentrations at the membrane surface, which can lead to spontaneous wetting of the membrane. A mass balance across the feed side boundary layer yields the relationship between molar flux, N_V, the mass transfer coefficient, k_f, and the solution concentrations (mole fractions), in the bulk feed (x_f), at the membrane surface (x_{fm}), and in the permeate (x_p) (Porter, 1972; Pusch, 1972)

$$\frac{N_V}{k_f c} = \ln\left[\frac{x_{fm} - x_p}{x_f - x_p}\right] \tag{24}$$

where c is the bulk liquid phase molar concentration. The method that is always used in the literature to determine the mass transfer coefficient is to employ the mass transfer analogy of the Dittus-Boelter equation

$$\frac{kd}{D_{AB}} = Sh = u\,\mathrm{Re}^s\,Sc^t \tag{25}$$

where D_{AB} is the ordinary diffusion coefficient of solute in water, u is a constant and Sh, Re, and Sc are the Sherwood, Reynolds, and Schmidt numbers. Various empirical correlations for different featured membrane modules are summarized in references (Lawson and Lloyd 1996b; Schoner et al., 1998; Costello et al., 1993; Schofield et al., 1990c).

4.2 Experimental Results and Discussion

4.2.1 N_2 Gas Permeation Measurements

The results of the N_2 gas permeance measurements are listed in tables 2a and 2b. The experiments yielded a result of 0.027 cubic centimeters per square centimeter

second centimeter of mercury ($cm^3/cm^2 \cdot s \cdot cm$ Hg) for module S/N 1004 and 0.05 $cm^3/cm^2 \cdot s \cdot cm$ Hg for module S/N 1005. These values are significantly lower than that of module MXFR #3 used in Phase II Project (Sirkar and Li, 2003) which was 0.196 $cm^3/cm^2 \cdot s \cdot cm$ Hg. The coatings on the fiber surfaces in both modules must be significantly tighter than those in MXFR #3 based on the data of N_2 permeance. In the experiment, the N_2 cylinder with a test gauge was connected to one end of the lumen side of the module. We believe that there was a much greater pressure drop along the fiber direction from the side connected with the gas cylinder to the other side. Therefore, the effective pressure difference between the tube side and the shell side for driving N_2 permeation through the membrane must have been lower than that indicated by the test gauge. The modules in Phase II Project and the small modules in this project had much shorter fibers and, therefore, the pressure drop was significantly lower. The present larger modules have fibers that are quite long. However, the measurement of N_2 gas permeation rate is still a very useful method for a rough characterization of the membrane properties and explaining the differences between different membrane coatings and their differing DCMD performances under similar experimental conditions.

4.2.2 DCMD Performances of Single Modules (Task 2)

4.2.2.1 Small Rectangular Crossflow Hollow-Fiber Membrane Modules

In the first quarter, five small rectangular modules having PP 50/280 fibers (280-μm I.D., 50-μm wall thickness) having different coatings were investigated. This was needed to facilitate the fiber selection in Task 1. The details of these five modules are shown in table 1a. Figures 10 and 11 display the variations of water vapor flux with feed brine interstitial velocities in the five membrane modules in MD. In VMD, the experimental details indicated in Phase II Project), the water vapor fluxes (figure 10) have a trend similar to the nitrogen permeation rate of these membranes (table 2a); this indicates that the process is limited by the transport of water vapor through the surface coating of membrane. This trend of the water vapor flux with respect to the membrane surface coating also appears to be valid for DCMD except for module MXFR #12 (figure 11). Generally, the more open the porous substrate for a giving coating, the higher the VMD flux and the DCMD flux. Compared to the uncoated membrane (in module MXFR #15), the ultrathin coating layers did not reduce the flux too much in the DCMD performance. This indicated an important progress. The coatings being used now by themselves do not reduce the water vapor flux very much. However, the water vapor fluxes obtained using this PP 50/280 fiber based rectangular module are low; these values are not competitive with those of the PP 150/330 hollow-fiber modules obtained in Phase II Project. These experiments guided us to select the right hollow-fiber membrane for the bigger modules being developed in Task 1 of the current project.

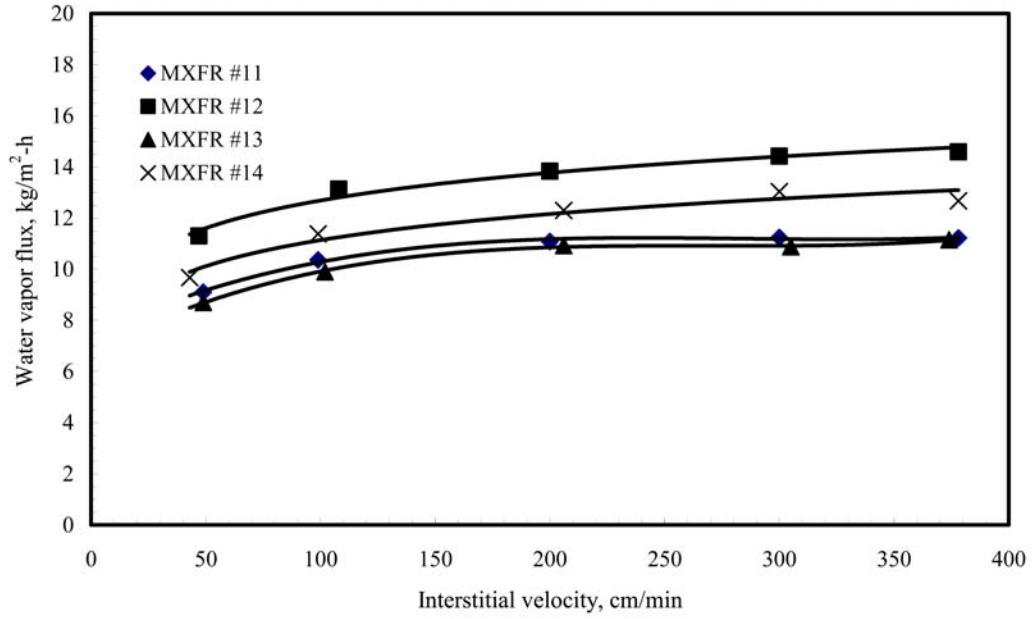

Figure 10. VMD: Variation of water vapor flux of membrane modules MXFR #11, MXFR #12, MXFR #13, and MXFR #14 with interstitial velocity of 1% brine as feed flowing through the shell side at 85 °C; tube side at a vacuum of 64-69 cm Hg.

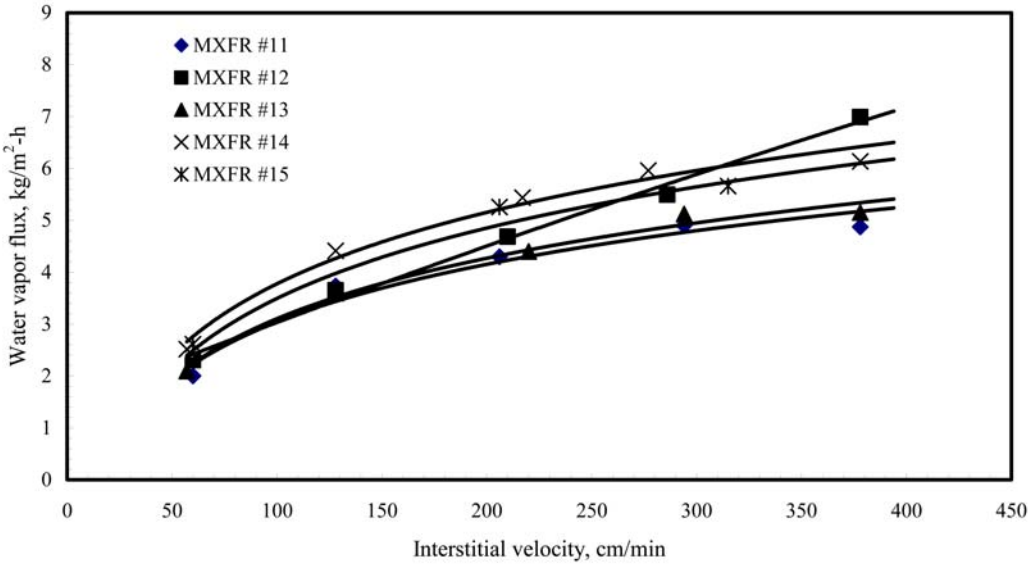

Figure 11. DCMD: Variation of water vapor flux of membrane modules MXFR #11, MXFR #12, MXFR #13, and MXFR #14 with interstitial velocity of hot brine (1% NaCl) as feed flowing through the shell side at 85 °C; (tube side: deionized water, 15-19 °C, linear velocity 770 centimeters per minute [cm/min]).

Table 2a. Characteristics of the Small Hollow-fiber Membrane Modules, Their Gas Permeation Properties, and Performances in VMD and DCMD

Particulars	[1]MXFR #9	[1]MXFR #10	MXFR #11	MXFR #12	MXFR #13	MXFR #14	MXFR #15
Support membrane type	PP 50/280						
Coating	Silicone fluoropolymer					Teflon	Uncoated
Shell-side flow mode	Crossflow						
[2]Permeance of N_2, cm^3 (STP)/cm^2·s cm Hg	0.011	0.009	0.018	0.024	0.017	0.020	0.018
[3]$F(VMD)_S$, kg/m^2·h (Re_d-shell)	7.2 (39)	6.8 (38)	11.1 (37.1)	13.8 (38.0)	10.9 (39.0)	12.3 (38.8)	–
[4]F(DCMD), kg/m^2·h	1.0	2.9	4.3	4.5	4.3	5.4	5.3
[5]Conductive heat flux (DCMD), kilocalorie per square meter second (kcal/m^2s)	5.6	5.8	6.3	7.7	6.5	6.4	6.2

[1] MXFR #9 and MXFR #10 were used in Phase II Project (Sirkar and Li, 2003).

[2] Experimental conditions: Temperature: 25.5 °C; atmospheric pressure: 76 cm Hg; N_2 inlet: tube side; N_2 outlet: shell side.

[3] $F(VMD)_S$: Water vapor flux (VMD), experimental conditions: brine (1% NaCl at 85 °C) as feed flowing through shell side at 200 cm/min of interstitial velocity; vacuum (60-66 cm Hg) at tube side.

[4] F(DCMD): Water vapor flux (DCMD), experimental conditions: shell side: 1% brine water at 85 °C (inlet temperature) at 200 cm/min of interstitial velocity; tube side: DI water at 15-17 °C (inlet temperature) at 766 centimeters per minute (cm/min) of linear velocity.

[5] Conductive heat flux = (heat transfer rate from the increase of temperature in the tube side - heat transfer rate for evaporation of water)/effective membrane surface area. It is supposed that the heat loss through the module faces in the tube side is negligible.

4.2.2.2 Larger Rectangular Crossflow Hollow-Fiber Membrane Modules

Two rectangular crossflow membrane modules, namely, S/N 1004 and S/N 1005 described in table 1b were used in this set of DCMD measurements. The relations between the temperatures and velocities of the feed and the distillate and the water vapor flux were investigated. The effect of the concentration of salt (NaCl) on the DCMD performances was also studied.

The variation of water vapor flux of module S/N 1005 with the interstitial velocity of hot brine feed (3%) entering the module at 85 °C is shown in figure 12, when the distillate inlet linear velocity was 1,560 centimeters per minute (cm/min). It was surprising that the water vapor flux did not increase with an increase of the feed velocity, but it decreased as the interstitial velocity of the hot feed was raised. From the experimental records, we found that the outlet temperatures of distillate from the module were 83-84 °C, which were very close to the feed inlet temperature.

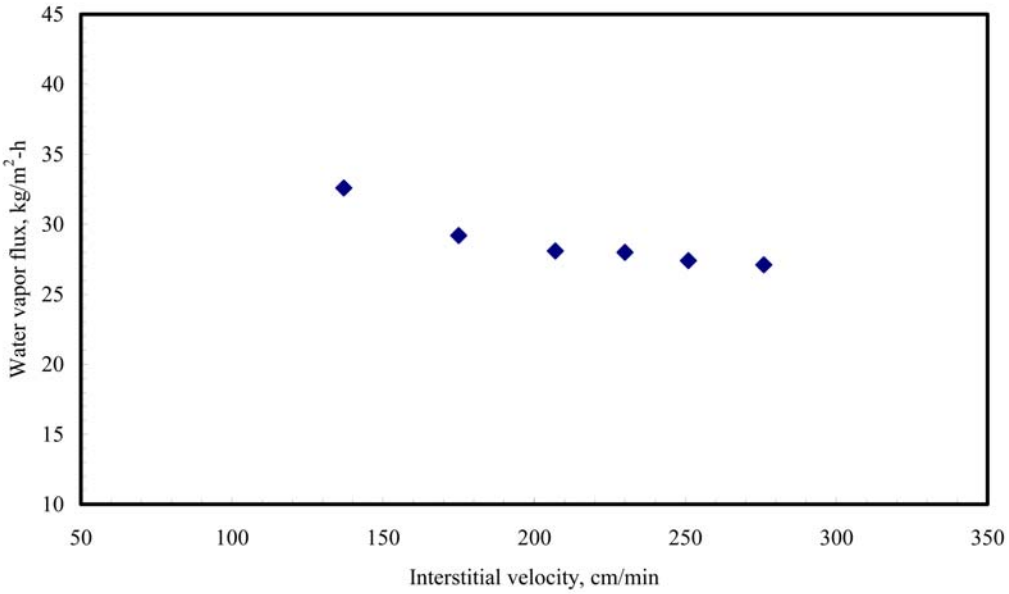

Figure 12. Variation of water vapor flux of module S/N 1005 with interstitial velocity of 3% brine flowing through shell side at a feed temperature of 85 °C and distillate entering the tube side with a linear velocity of 1,560 cm/min at 16 °C.

Compared to the module MXFR #3 used in Phase II Project, we realized that the fibers in the current modules S/N 1004 and S/N 1005 are substantially longer (four times). The heat transported by water vapor and conducted through the membrane material was excessive; it reduced the temperature difference between the shell side and tube side of the membrane which is the driving force of the DCMD process. So, the effect of hot brine velocity (also the brine-side boundary layer heat transfer coefficient) on the water vapor flux, which was found to be very important in Phase II Project, would not be important until a lower distillate outlet temperature is provided. Therefore, how to improve the operational conditions to decrease the outlet temperature of distillate was our first objective to improve the DCMD performance of the big membrane module. To that end, the effect of linear velocity of the distillate on the water vapor flux was investigated. The results are shown in figure 13.

It can be seen from figure 13 that the distillate outlet temperature decreased with an increase of linear velocity of distillate due to the decrease of the residence time of distillate in the module, which led to an increase of the driving force for water vapor permeation due to increasing ΔT (T_{brine}-$T_{distillate}$). This led to a higher water vapor flux. Also, an increase of linear velocity in parallel flow on the tube side led to an increase of Reynolds number which maximized the distillate-side boundary layer heat transfer coefficient. Higher heat transfer coefficient leads to a lower temperature at the distillate-membrane interface which supports the increased water vapor flux. We observed in module S/N 1004 a water vapor flux

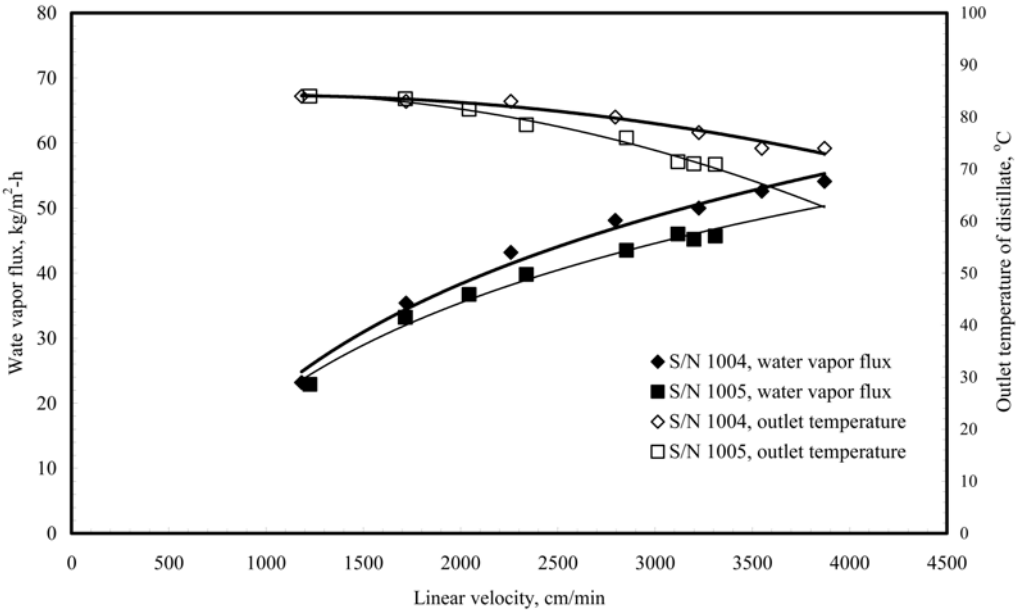

Figure 13. Comparison of DCMD performances of modules S/N 1004 and SN 1005: variation of water vapor flux with inlet linear velocity and outlet temperature of distillate flowing through the tube side at inlet temperatures of 16-24 °C and 3% brine at 85 °C flowing on the shell side at 25 L/min (interstitial velocity of 230 cm/min).

value of around 54 kg/m^2·h, the level achieved in Phase II using an order of magnitude of smaller module, when the linear distillate velocity was 3,900 cm/min. However, the water vapor flux of the larger module is somewhat lower than that of small module MXFR #3 used in Phase II. The resistance to water vapor diffusion through the membrane from the outside surface coating of fibers is one of the most important factors to affect the water vapor flux; this is potentially reflected in the N_2 permeances measured in section 4.2.1. We also notice that at low linear velocity of distillate in the fiber lumen, e.g., 1,200 cm/min, the outlet temperature of distillate reached 84 ^{o}C, which means that there was essentially no temperature difference across the membrane since the feed inlet and outlet temperatures were from 84.5-85 ^{o}C. Even if the distillate linear velocity was as high as 3,800 cm/min, the distillate outlet temperature still was 74 ^{o}C or higher for module S/N 1004. These results will allow us to improve our design and experiments in future.

A variation of the water vapor flux with feed inlet temperature is illustrated in figure 14 for city water, 3% brine, 6% brine, and 10% brine. Normally the feed temperature has a small effect on the Reynolds number at a given flow rate. That is because there are only limited changes in the density and the viscosity of water in the given temperature range. But the effect of temperature on the water vapor permeation flux is striking in our situation. The increase of the feed temperature

increases the Reynolds number a little bit, but it drastically increases the water vapor pressure which is the driving force. That is why the water vapor flux rises almost exponentially with temperature as the brine temperature rises.

It is very important to know how our membrane system works with different brine solutions as feed under the current experimental conditions. In Phase II Project, a set of VMD experiments was carried out with DI water and 1% brine as feed flowing on the shell side of membrane module to illustrate the effect of salt concentration in the feed on water vapor flux. It was concluded that the effect of salt concentration over this performance was negligible under the VMD experimental conditions when the salt concentration was increased to 1%. It is also very necessary to investigate the behaviors of our membranes working with more highly concentrated salt solutions under DCMD conditions for testing its overall usefulness. A group of DCMD experiments was conducted to determine the effect of NaCl concentration on the water vapor flux in our current large rectangular crossflow membrane module system. The experimental data shown in figure 14 and figure 15 do not provide any conclusive evidence that increasing the NaCl concentration of the feed to 10% of NaCl reduces the system performance too much. This is obvious since water vapor pressure is affected to a small extent by salt concentration, which can be explained by using equations (21), (22), and (23). When salt concentration in water is 10%, $p_i / p_0 = 0.94$; when salt concentration reaches 20%, $p_i / p_0 = 0.85$. The crossflow of hot feed on the

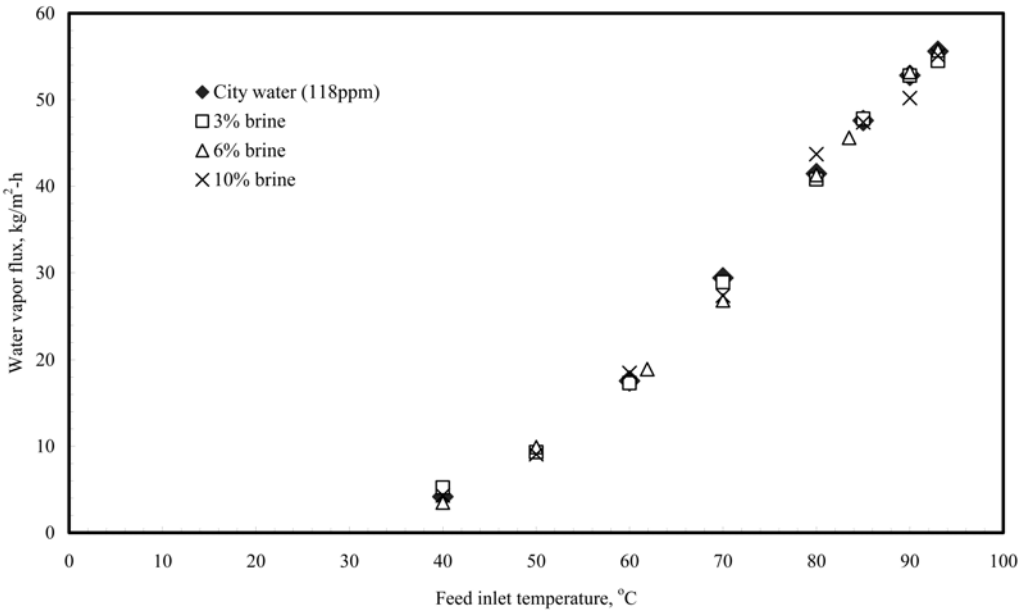

Figure 14. DCMD performance of module S/N 1004 (membrane surface area: 2,864 cm^2) with city water, 3% brine, 6% brine, and 10% brine as feed solutions: variations of water vapor flux with feed inlet temperature (shell side: brine solution at 230 cm/min of interstitial velocity; tube side: distillate at 2,850 cm/min of average linear velocity at 25-35 °C of the inlet temperature).

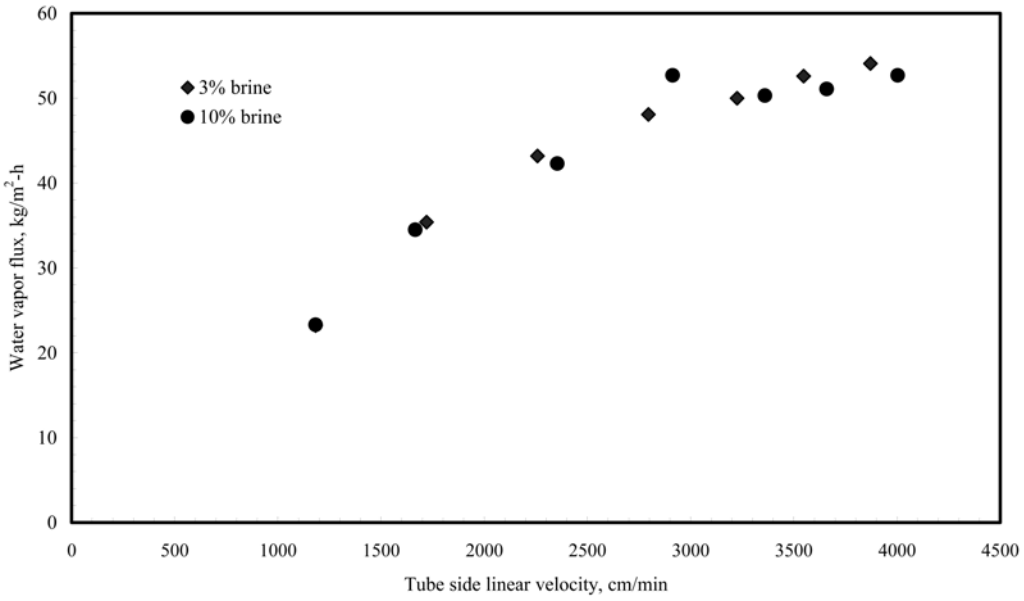

Figure 15. DCMD performance of module S/N 1004 (membrane surface area: 2,864 cm^2) with 3% brine and 10% brine as feed solutions: variations of water vapor flux with linear velocity of distillate flowing through the tube side at linlet temperatures of 18-26 °C and hot brine flowing on shell side with 25 L/min (interstitial velocity of 230 cm/min) at a temperature of 85-88 °C.

shell side is also a very important contributing factor which could reduce the concentration and temperature polarizations to a great extent. These results point out that this DCMD technology may be used to successfully recover water at a high rate from highly concentrated salt solutions, e.g., the rejected hot seawater/the hot brine blowdown from a thermal distillation plant. It also suggests how the concentrate volume from existing plants may be reduced and more water recovered.

Figure 16 illustrates how the distillate inlet temperature affects the DCMD performance of module S/N 1004. Water vapor flux obtained has been plotted for a 3% brine feed at 91-93 ^{o}C flowing on the shell side at an interstitial velocity of 230 cm/min and distillate flowing on the tube side at a linear velocity of 2,950 cm/min as a function of the distillate inlet temperature. In this figure, the variation of distillate outlet temperature with the distillate inlet temperature has also been shown. As the inlet distillate temperature is increased, the driving force of the DCMD process is decreased and therefore the water vapor flux decreases. It can be seen during this experiment that the distillate outlet temperature was just raised by 4 ^{o}C (from 88-92 ^{o}C, very close to the feed inlet temperature) even as the distillate inlet temperature was varied from 30-60 ^{o}C. This indicates that we still have an opportunity to get higher water vapor flux in future by optimizing the

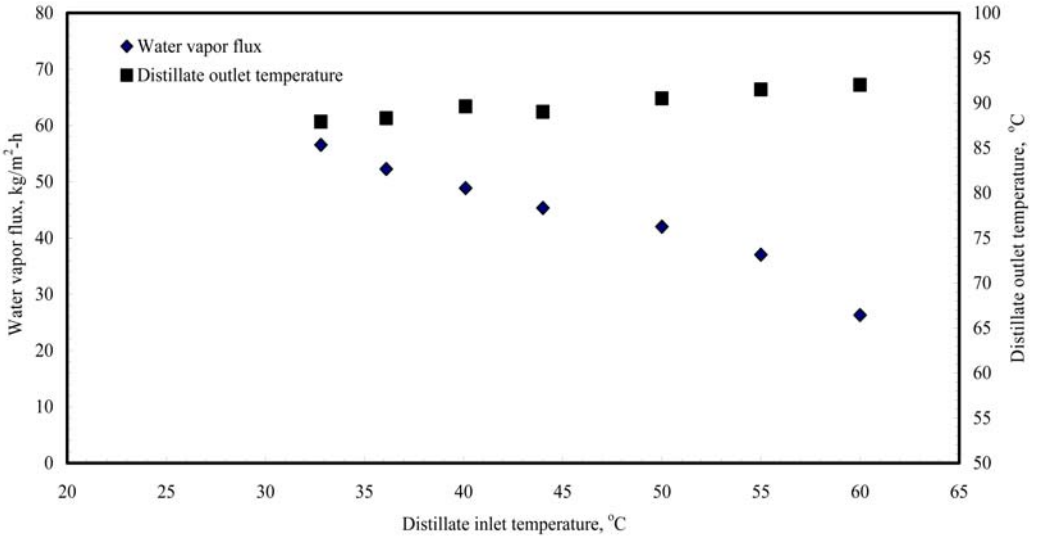

Figure 16. DCMD performance of module S/N 1004 (membrane surface area: 2,864 cm^2): variation of water vapor flux with distillate inlet temperature (shell side: 3% brine at 230 cm/min of interstitial velocity at a temperature of 91-93 °C; tube side: distillate at 2,950 cm/min of linear velocity): variation of distillate outlet temperature with the distillate inlet temperature has also been shown.

experimental operations even if the water vapor flux has already reached 56.5 kg/m^2·h in the current study. We also found that a very high water vapor flux of 42 kg/m^2·h was obtained although the inlet temperature of distillate was as high as 55 °C.

4.2.3 DCMD Experiments for an Extended Period (Task 2)

Membrane module S/N 1004 was employed for an extended DCMD run in Task 2 in August 2003. A feed of 3% hot brine was circulated through a microfilter, the shell side of module S/N 1004, and the feed reservoir. Similarly, cold DI water was recirculated as the distillate stream through a microfilter, the lumen, the distillate reservoir, and the thermostat shown in figure 6a. Figure 17 represents the variation of water vapor flux with the operating time. For a brine feed at a temperature of 87-90 ^{o}C, this experiment lasted 5 days. The water vapor flux of the membrane dropped very slowly until the experiment was run for 100 hrs. The stable water vapor flux was 54 kg/m^2·h. There was a reduction of only 6% in the water vapor flux. Compared to the membrane module MXFR #3 measured in the Phase II project (a reduction of 23% during the 5-day-long term experiment), the 6% reduction is much smaller. Although the role of the thermal creep in the membrane and coating material with time around the mouth of the partially covered pore at a high temperature cannot be eliminated, the fouling of the membrane both on the shell-side and the tube-side surfaces was inhibited effectively by microfiltration (1 μm). The conductivity of the cold distillate was monitored during this extended experiment. The concentration of salt was always

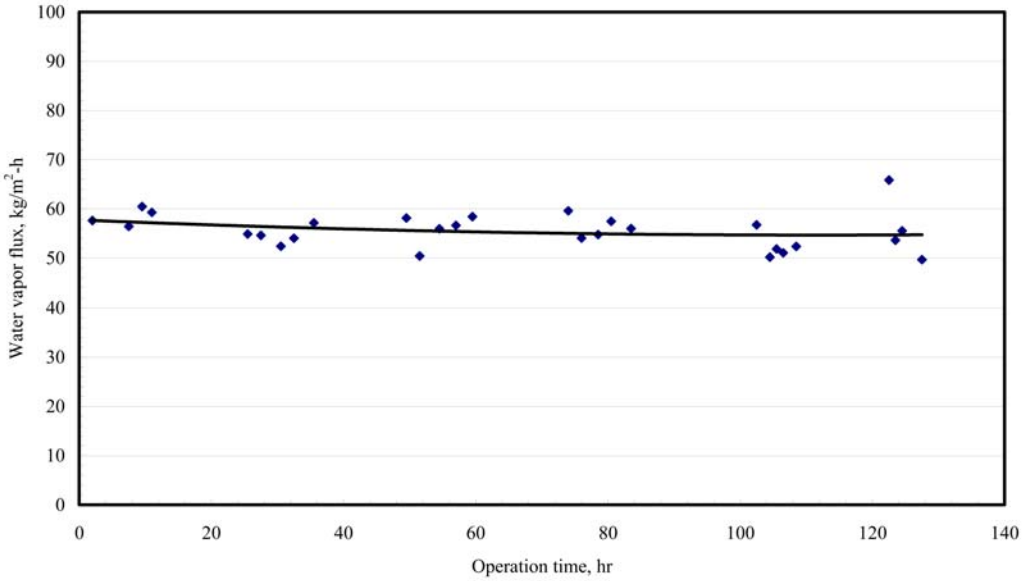

Figure 17. Variation of water vapor flux with operating time for hot brine (3% NaCl) recirculating through the shell side with an inlet linear velocity of 253 cm/min (Reynold number, 78) at 87-90 °C, and cold distillate water recirculating through tube side at an inlet velocity of 3,870-4,060 cm/min (Reynolds number, 448-471) at an inlet temperature of 34-42 °C (module S/N 1004).

less than 10 milligrams per liter (mg/L), which indicates that the membrane pores were not wetted by the hot brine during this experiment. No bacterial stain was observed in the membrane module or the brine reservoir during the 5-day experiment. Generally, bacterium can not grow in water at the temperature over 85 ^{o}C. However, the pressure drop in the cold distillate water passing through the lumen side of the module was slightly increased (by 8%). This indicates the possibility of dirt buildup in the hollow-fiber tube sheet.

A note about the mode of operation during the long-term test is in order. The experiments were started in the morning at 8 a.m. with 87-90 °C brine feed on the first day; then at about 8 p.m. in the evening the hot feed temperature was reduced to 50 °C. Next morning at 8 a.m., the hot feed temperature was increased again to 87-90 °C; at 8 p.m. in the evening, the hot feed temperature was reduced again to 50 °C. The water vapor fluxes reported correspond to the high-temperature feed during the first 12 hr of the day during the 5-day period. The brine Reynolds number employed was 78.

Membrane module S/N 1004 was used for a cumulative time of around 300 hrs since June 2003 and continuously over a period of 5 days/127 hrs. Until the end of August 2003, it was continuously used for DCMD tests. No leakage was observed. The silicone-fluoropolymer coating provides an effective barrier to protect the membrane. The membrane performance demonstrated very good stability and also indicated that this scaled-up module can perform as well as the

much smaller module MXFR #3 of Phase II both in terms of water vapor flux and distillate water quality.

4.2.4 DCMD Performances of a 2-Module Stack (Task 3)

As described in Task 2, the DCMD performances of a single larger module were investigated systematically. In this section, the behavior of a 2-module stack in DCMD will be reported.

Figure 18 illustrates the variation of water vapor flux of a 2-module stack (total membrane surface area: 5,728 cm^2) with inlet temperature of 3% brine flowing on the shell side at an interstitial velocity of 230 cm/min when two larger modules S/N 1004 and S/N 1005 were placed back-to-back. The water vapor flux increases with an increase of the inlet temperature of brine nearly in a straight line. Compared to the single module, the 2-module stack has a water vapor flux similar to that of a single module at low inlet temperatures of feed (below 50 °C). As the feed inlet temperature is increased, the difference of water vapor flux between the single module and the stack becomes larger so that the water vapor flux of a single module is higher than that of the stacked module by 12 $kg/m^2 \cdot h$ at

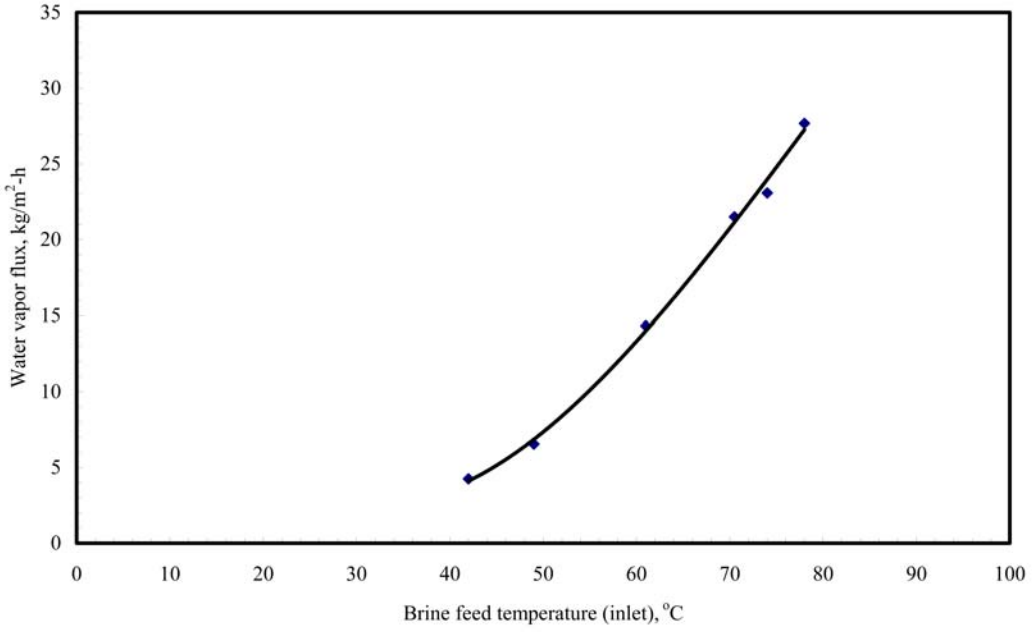

Figure 18. Variation of water vapor flux of stacked modules S/N 1004 (outlet) and S/N 1005 (inlet) (total membrane surface area 5,728 cm^2) with inlet temperature for 3% brine as feed flowing through shell side at an interstitial velocity of 230 cm/min and distillate flowing on the tube side with a linear velocity of 3,000 cm/min at inlet temperatures from 24-50 °C.

80 °C of feed inlet temperature. As can be seen, in the experiment with the stacked module, hot brine exiting one module at a temperature lower than the feed brine temperature enters immediately the next module. Since the effective brine temperature in the next module is lower, the water vapor flux achieved is also lower.

To improve the DCMD performance of the stacked module, another experiment was carried out by increasing the feed interstitial velocity to overcome the lower inlet temperature of the feed entering the second module. The experiment did not give us the expected result (figure 19). The water vapor flux was not increasing a lot with an increase of feed interstitial velocity. This suggested that the lower feed inlet temperature for the second module did not lead to a substantial decrease of driving force for the water vapor permeation; to understand this result we checked the experimental record for a single module. When the feed interstitial velocity was in the range of 150-280 cm/min, the temperature difference between the upside and the downside of a module was 1-3 °C, which cannot lead to a big reduction in the driving force. As indicated in Section 4.1.2, "Experimental Apparatus and Procedures," the cooling capacity of the chiller we currently are using is 12 kW, which is not enough to cool down the hot distillate coming from the stacked module to the expected temperature. That leads to a very high distillate inlet temperature. Therefore, the temperature difference between the feed and distillate must be very low and, thus, the water vapor flux should be low.

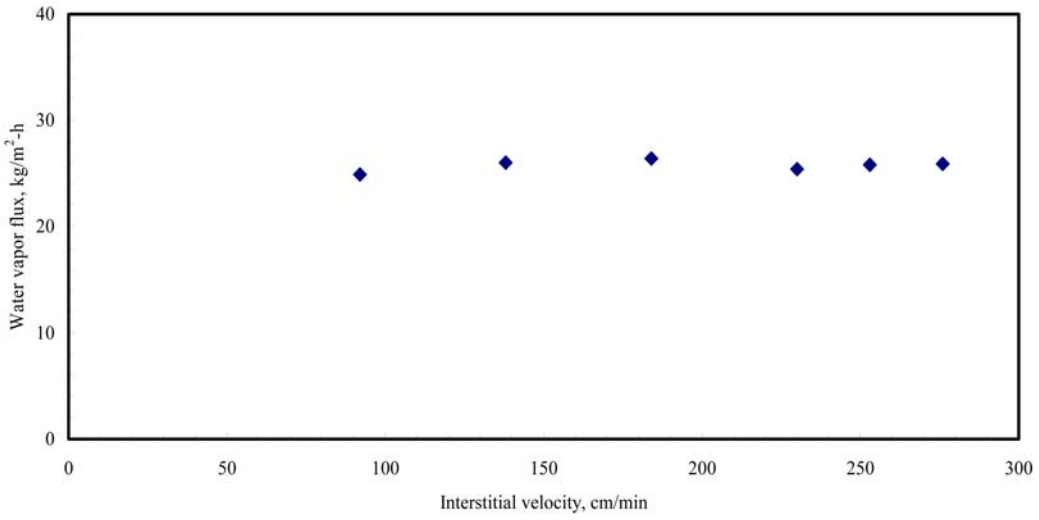

Figure 19. Variation of water vapor flux of stacked modules S/N 1004 (outlet) with interstitial velocity of 3% brine flowing through the shell side at inlet temperatures from 81-75 °C and distillate flowing on the tube side with a linear velocity of 3,120 cm/min at inlet temperatures from 28-50 °C.

The DCMD performance of the stacked module should be improved to a great extent when the cooling system is improved. However, these experiments illustrate how one can stack the horizontal crossflow modules in a small volume and extract as much water vapor as possible from a given hot brine stream.

4.2.5 Electron Micrographs of Coated Fibers

Interpretation of the N_2 permeances (in section 4.2.1) and their corresponding water vapor fluxes of fibers having different coatings can be facilitated by electron micrographs of the coated fiber surfaces. Since we did not want to damage the successful modules of the Phase II research and this project, we selected fibers from modules which were not used due to excessive leakage at the tube sheet potting. The modules selected were: MXFR #2 (Phase II) and S/N 1002 (this project). The base fibers in both modules were identical PP 150/330 fibers from Membrana. The coatings on these fibers were close (according to AMT) but not identical. The N_2 permeance values were:
0.153 cm^3 (STP) /cm^3/cm^2·s·cm Hg for MXFR #2 (Phase II) and
0.070 cm^3 (STP)/cm^3/cm^2·s·cm Hg for S/N 1002 (table 2b).

Figures 20a and 20b illustrate the electron micrographs of the surface on the outside diameter of the fibers for MXFR #2 and S/N 1002 modules, respectively. One can see that the openings on the surface of fibers in S/N 1002 are smaller and less numerous than those in MXFR #2. Correspondingly, S/N 1002 has lower N_2 permeance. We expect that such change in the microporous coating morphology will be reflected not only in the N_2 permeance but also in the water vapor permeance. The substrate pore sizes are smaller and visible through the coating in figure 20a.

4.2.6 Comparison of Data from S/N 1004 and MXFR #3 for Scale-Up Considerations

Table 3 illustrates the comparative DCMD performances of modules S/N 1004 and MXFR #3. What we observe is that even though module S/N 1004 has a membrane surface of 0.29 m^2 compared to 0.012 m^2 for module MXFR #3, the water vapor fluxes of the two modules are not far apart for almost similar experimental conditions. The somewhat lower flux of S/N 1004 is due to the less porous nature of the coating on the fibers in S/N 1004 compared to that in MXFR #3.

Table 2b. Nitrogen Permeation Properties and DCMD Performances of the Larger Hollow-Fiber Membrane Modules

Particulars	S/N 1002	S/N 1003	S/N 1004	S/N 1005	[1]MXFR #3
Shell side flow mode	Crossflow				
Permeance of N_2,[2] $cm^3(STP)/cm^2 \cdot s \cdot cm$ Hg	0.070	0.070	0.027	0.050	0.196
DCMD performance (below):[3]					
N_V,[4] $kg/m^2 \cdot h$	--	--	23.3	22.9	41.4
Re_T (tube side)	--	--	118	122	68
Re_S (shell side)	--	--	71	72	58
Pressure drop (tube side)[5], kilopascal	--	--	11.5	11.7	6.9
η [6]	--	--	0.44	0.42	0.65

[1] MXFR #3 data from Phase II Project (Sirkar and Li, 2003) included here for comparison.
[2] Experimental conditions: 25.5 °C, 76 cm Hg; N_2 inlet: tube side; N_2 outlet: shell side.
[3] DCMD for MXFR #1 and MXFR #3: shell side: 1% saline water at 85 °C (inlet temperature) at 200 cm/min of interstitial velocity; tube side: DI water at 15-17 °C (inlet temperature) at 760 cm/min of linear velocity. DCMD for S/N 1004 and S/N 1005: shell side: 3% saline water at 85-88 °C (inlet temperature) at 235 cm/min of interstitial velocity; tube side: DI water at 20-24 °C (inlet temperature) at 1,200 cm/min of linear velocity. DCMD was not performed for modules S/N 1002 and S/N 1003 due to tube-sheet leakage.
[4] N_V : Water vapor flux.
[5] Pressure drop of cold distillate on the tube side along the module length.
[6] η : Evaporation efficiency.

Table 3. Comparison of Data from S/N 1004 and MXFR #3 for Scale-Up Considerations

	Shell side (feed, brine)				Tube side (distillate water)			
Module	NaCl concentration %	Inlet temperature °C	Outlet temperature °C	Interstitial velocity cm/min	Inlet temperature °C	Outlet temperature °C	Linear velocity cm/min	Flux $kg/m^2 \cdot h$
MXFR #3	1	90.1	86.6	231	18.1	62	1,650	79
S/N 1004	3	88.3	82.1	276	36	73	4,360	[1]60

[1] N_2 permeation data indicate the coatings in the hollow fibers of modules S/N 1004 and S/N 1005 to be less porous than those in the fibers of MXFR #3 (table 2b).

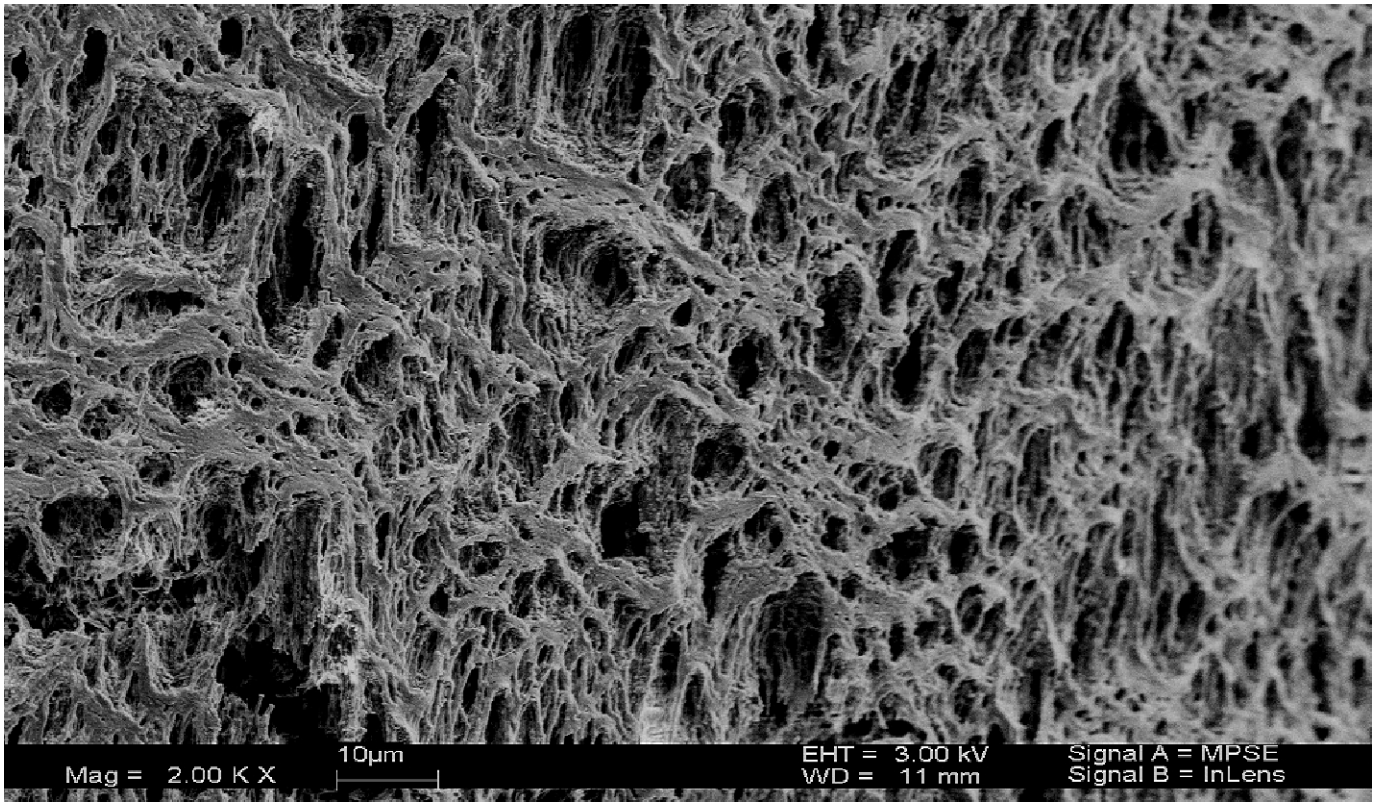

Figure 20a. SEM photograph of coating on the fibers of module MXFR #2; N_2 permeance: 0.153 $cm^3/cm^2 \cdot s \cdot cm$ Hg.

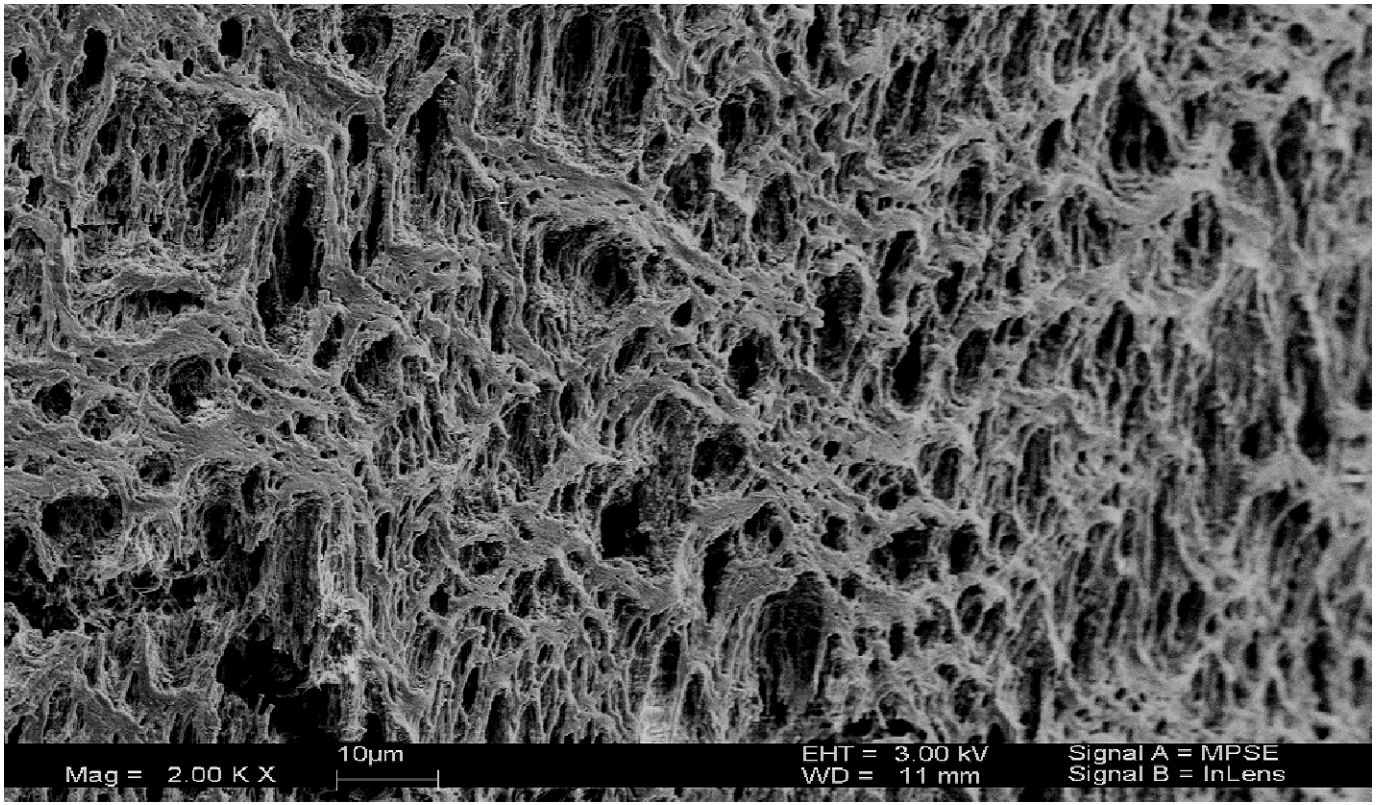

Figure 20b. SEM photograph of coating on the fibers of module S/N 1002; N_2 permeance: 0.070 $cm^3/cm^2 \cdot s \cdot cm$ Hg.

4.2.7 Cost Estimate (Task 5)

A brief comparison of seawater desalination by reverse osmosis and the proposed direct contact membrane distillation process with respect to the production cost is provided in this section. For our basis of calculation, we assume a purified water production rate of 1,000,000 gal/day (3,800 cubic meters per day [m^3/day]). The values for RO are taken from Ray (2001). Other references include Peters and Timmerhaus (1991) and Mulder (1991).

The calculation of production cost is normally based on the capital cost and operating cost. The cost categories for capital and operating costs used in this estimation are shown in table 4. For the comparison between RO and DCMD, the following assumptions were employed.

(1) Both RO and DCMD desalination plants have the same production rate—1,000,000 gpd.

(2) RO: operating pressure 1,000 psi, 30% recovery, feed flow rate 2.3 thousand gallons per minute (kgal/min) (=0.15 cubic meters per second [m^3/s]), energy recovery 30%.

DCMD: shell side operating pressure 10 psi, 12% recovery, feed flow rate 5.66 kgal/min (=0.36m^3/s).

(3) The costs of some capital items—site development, water, utilities, construction overhead and contingency, and some operating costs—membrane replacement, labor, spare parts, and filters in RO application are the same as those in DCMD.

(4) Both RO membrane and DCMD membrane have the same price (dollars per square meter [$/$m^2$]). The permeation flux of DCMD is 1.5 times higher than RO. Estimated membrane lifetime is 3 years.

(5) In DCMD, there are two special situations:

(a) An initial amount of cooled distillate water flows on the distillate side. This water gets heated up as it collects the condensate. A fraction of this heated distillate is taken out as product. The rest is cooled in a heat exchanger by cooling water which is cooled down again by means of a cooling tower. Thus additional costs involved include those of □ distillate heat exchanger; □ cooling tower and □ cooling water lost by evaporation in cooling tower.

(b) On the hot brine side, the exiting hot brine temperature is sufficiently lowered. An amount of fresh brine is added to it and then this brine is heated up in a heat exchanger by the waste heat source so that it can be fed again to the membrane

stack. We have assumed 30% recovery; we can go for even higher recovery. However, it will require a few passes. The costs involved are brine heat exchanger; additional pumping cost. When waste heat is not available, the energy for heating the saline water has to be added. We have incorporated it here — $0.85/kgal.

The values in table 4 indicate that the total production cost of water by DCMD process is $3.63/kgal, which is significantly lower than that by RO process due to the low-pressure operation of DCMD process, high water vapor flux, and good anti-fouling properties of the DCMD membrane and process. Compared to the RO process widely used in desalination industry, the salt content of water made from our current DCMD system is less than 20 parts per million (ppm), but the salt content in water got from single-stage RO system is greater than 200 ppm. Therefore, it is prospective to apply the novel technology in large-scale desalination.

Note: recent cost reports for water treatment process showed that the production cost of water by RO was $4.77/kgal (Cost Model, Program for PC, D-8230, Water Desalination and Water Purification Research and Economic Program, Reclamation's Web site, http://www.usbr.gov/water/desal.html, 2002-2003).

4.2.8 Information About Potential Pilot Plant Studies in the Future (Task 6)

The major requirements for the location of a pilot plant at a given site are: accessible and availability of (1) hot saline water, (2) power, (3) limited amount of fresh water, (4) brine concentrate disposal facility and (5) site engineering capability. Among a number of sources of hot brines for potential use in such a project, the geothermal sources in Tularosa Basin in New Mexico or in California are of interest. The following information and suggestions have been provided by Dr. Michael Hightower of Sandia National Laboratory, Albuquerque, N.M. (Tel. 505-844-5499; mmhight@sandia.gov) regarding the Tularosa Basin Research and Development Center (TBRDC). The geothermal wells in Tularosa Basin yield saline water containing 3,000-10,000 ppm total dissolved solids (TDS) at 50-70 °C. There are adjoining solar heating facilities. The geothermal water may be heated up in the solar heating facilities to 85-95 °C for use as the brine feed to the DCMD pilot plant. This will allow the achievement of a much higher water vapor flux as well as a higher fractional extraction of water. However, as figures 14 and 18 illustrate, 70 °C feed brine may also be used; a lower water vapor flux level of around 20-30 $kg/m^2 \cdot h$ will be achieved.

Table 4. Summary of Representative Costs for RO Treatment and DCMD Treatment

Cost category	RO[1]	DCMD
Capital Costs (dollars per gallon per day [$/gal/day])		
Direct		
Site development	0.10	0.10
Water	0.09	0.09
Utilities	0.16	0.16
Equipment[2]	3.34	2.04
Land[3]	---	---
Other	---	---
Total direct capital costs	3.69	2.39
Indirect		
Construction overhead	0.44	0.44
Contingency	0.37	0.37
Other	---	---
Total indirect capital costs	0.81	0.81
Total capital costs	4.50	3.20
Operating Costs (dollars per thousand gallons [$/kgal])		
Energy[4]	1.34	0.25
Membrane replacement	0.41	0.41
Labor and overhead	0.30	0.30
Spare parts	0.09	0.09
Chemicals	0.16	0.08
Filters	0.05	0.05
Cooling water	---	0.10
Exhaust steam[5]	---	0.85
Other (ion exchange beds)	---	---
Total operating costs	2.35	2.13
Capital recovery costs[6]	2.13	1.50
Total production costs ($/kgal)	4.48	3.63

[1] Quoted from Ray in *Membrane Handbook* (2001), p. 368.
[2] Categories of equipment costs ($/gal/day)

Component	RO	DCMD
Pretreatment①	0.5	0.3
Membrane module	0.5	0.35
Pumps②	0.8	0.04
Controls, pressure vessels, electrical subsystems, heat exchangers, power recovery system③	1.2	1.01
Shipping and installation	0.17	0.17
Equipment related engineering	0.17	0.17
Total	3.34	2.04

① Pretreatment cost of seawater for DCMD is much lower than that for RO because almost no chemical treatment is needed in DCMD application.

② Reference: Bureau of Reclamation letter (Denver Federal Center) on June 23, 1999.

③ Here we have found that the cost of all items except energy recovery system (used in RO process) is $0.6/gal/day. The cost calculations for heat exchangers and cooling tower (used in DCMD process) are based on the most recent experiments.

The stable (average) water vapor flux: 40 $kg/m^2 \cdot h$; total membrane area for the production of 1 million gallons per day: 157,708(kg/h)/40($kg/m^2 \cdot h$)=3,943m^2; total number of modules (each module composed of 4 current modules in series, $4 \times 0.2864 = 1.146 m^2$/module): 3,943($m^2$)/1.146 ($m^2$/ module)=3,440; feed flow rate on the shell side (four modules in series in DCMD process): (3,440÷4)×25(L/min) = 21,500(L/min) = 0.36(m^3/s); distillate flow rate on the tube side: 3,440×(2.6×4)(L/min) = 35,800 (L/min) = 9,460(gpm) = 0.6(m^3/s). (Module area calculation and flow rates based on projection from present system).

(a) Cost of cooling tower: $0.2 million (Peters and Timmerhaus (1991), Figure B-6, page 810). Cost of cooling water $0.10/kgal (Peters and Timmerhaus (1991), Table 5, page 815).

(b) Cost of heat exchangers

Feed-shell side: brine water would be heated from 70 °C to 90-95 °C by steam through this heat exchanger if we need to extract more water by multipass arrangement. This is not needed for single pass.

Heat flux: 21,500(L/min)×1,000(g/L)×20(^{o}C)×1(cal/g ^{o}C) = 1×10^{8} (British Thermal Units per hour [BTU/h]) (Note: 1BTU = 252cal). Assume overall heat transfer coefficient = 500 BTU/h-ft^{2}-^{o}F (Peters and Timmerhaus (1991), Table 6, page 601).

Surface area of heat exchanger: 1×10^{8}(BTU/h)/(500(BTU/h-ft^{2}-^{o}F)×27(^{o}F)) = 7×10^{3} ft^{2} (Temperature difference: 27 ^{o}F)

Cost: $\$0.6\times10^{5}$ (Peters and Timmerhaus (1991), Figure 15-14, page 616)

Distillate-shell side: distillate would have to be cooled from 85 ^{o}C to 30-40 ^{o}C by cold water from the cooling tower.

Heat flux rate: 35,800(L/min) × 1,000(g/L) ×50(^{o}C) ×1(cal/g ^{o}C) = 4.2 ×10^{8}(BTU/h)

Surface area of heat exchanger: 4.2×10^{8}(BTU/h)/(400(BTU/h-ft^{2}-^{o}F)×90(^{o}F)) = 1.2×10^{4} ft^{2}

(Note: overall heat-transfer coefficient from water to water = 400(BTU/h-ft^{2}-^{o}F); average temperature difference: 90 ^{o}F.)

Cost: $\$1.5\times10^{5}$ (Peters and Timmerhaus (1991), Figure 15-14, page 616)

Total capital cost for the cooling tower and heat exchangers: $\$(2+0.6+1.5)\times10^{5} = \$4.1\times10^{5}$

The cost in \$/gal/day: 4.1×10^{5}(\$)/10^{6}(gal/day)) = \$0.41/gal/day

[3] Normally the land-related costs are negligible.

[4] Energy costs include costs for pumps for feed well, high-pressure pumps, cooling, heating, pretreatment system and instrumentation. Suppose industrial waste heat is available; the heat cost can be neglected in DCMD. The dominant energy cost in most installations is for the high-pressure pumps in RO applications; DCMD pumps are cheap low pressure centrifugal pumps. The representative energy costs can be calculated for a single-stage system using the equation

$$E_P = \frac{q_v \Delta P}{\eta}$$

where q_v = flow rate (m^3/s); ΔP = pressure difference (Pa); η = efficiency of pump and motor (%)

RO: consumption of energy

$$E_0 = \frac{1000(psi)\times 6.9\times10^{3}(Pa/psi)\times 0.15(m^3/s)}{0.65} = 1592(kW)$$

Recovery of energy = 1,592(kW) × 30% = 477.6 (kW)

So the total energy consumption = 1,592(kW) – 477.6(kW) = 1114.4 (kW)

Energy cost of 1,000 gallons water produced =

$$\frac{1114.4(kW)\times 24(hr)\times 0.05(\$)}{1000(gallon)} = 1.34(\$)/kgallon$$

Here pressure difference = 1000 psi; 1 psi=6.9 × 10^{3}Pa; η = 0.65; electricity price = \$0.05/(kW·hr).

DCMD: (1) Feed and distillate flowing through the membrane modules:

Shell-side consumption of energy for 10 psi pressure drop

$$E_0 = \frac{10(psi)\times 6.9\times10^{3}(Pa/psi)\times 0.36(m^3/s)}{0.65} = 38.2(kW)$$

Energy cost of 1,000 gallon water produced =

$$\frac{38.2(kW)\times 24(hr)\times 0.05(\$/kW\cdot hr)}{1000(gallon)} = 0.046(\$)/kgallon\cdot$$

Based on a similar calculation, the energy cost of distillate flowing on tube side is found to be $0.04/kgal.

Here the pressure drop on tube side is 5 psi and on shell side is 10 psi.

(2) Heat exchangers and cooling tower

For the heat exchanger for the shell side brine, only one side needs pump due to low pressure waste steam placed on the other side. The maximum energy cost is $0.05/kgal.

For tube side heat exchanger, it is supposed that the flow regimes are similar to the DCMD membrane modules. Therefore, the energy cost for both shell and tube sides should be $0.05 + $0.04 = $0.09/kgal.

For the cooling tower, operating pressure should be much lower than those of heat exchangers. It is reasonable to set the energy cost equal to $0.02/kgal.

Total cost for energy: $0.25/kgal.

[5] Calculation of waste heat cost for producing 1,000 gallon distillate water

(Latent heat of water: 540 cal/g; Specific heat of water: 1 cal/g/^{o}C; Specific heat of super-heated steam: 0.49 cal/g/^{o}C; Cost of exhaust steam: $0.8-1.5/klb = $6.7-12.5/kgal [+])

[+] Max S. Peters and Klaus D. Timmerhaus, Plant Design and Economics for Chemical Engineers, 4th Edition, McGraw-Hill, Inc., (1991), Table 5, page 815

The estimated feed outlet temperature is around 65-70 ^{o}C when 4 modules are in series and feed inlet temperature is between 90 and 95 ^{o}C. The distillate outlet temperatures of the first two modules are as high as 80-85 ^{o}C which can be used to heat the outlet feed solution from 70-80 ^{o}C via a heat exchanger. Heat flow rate for producing 1000 kgal distillate water/day on the tube side provided by steam for warming feed from 80-90 ^{o}C should be:
0.36 $m^3/s \times 10^6$ $g/m^3 \times$ (90-80)^{o}C × 1 cal/g/ ^{o}C ÷ 252 cal/BTU = 1.4×10^4 BTU/s

Heat needed to produce 1 kgal distillate on the tube side:
1.4×10^4 BTU/s × 24 h/day × 60 min/h × 60 s/min ÷ 1000 kgal = 1210 kBTU/kgal

Heat released from 1 kgal 120 ^{o}C steam condensing to 70 ^{o}C hot water:
1000 gal × 3.8 kg/gal × 1,000 g/kg × (0.49 cal/g/^{o}C × (120 ^{o}C – 100 ^{o}C) + 540 cal/g + 1 cal/g/^{o}C × (100 ^{o}C – 70 ^{o}C))/252 cal/BTU = 8,740 kBTU

Therefore, producing 1 kgal distillate on the tube side needs steam
1,210 ÷8,740 = 0.138 kgal

Cost of steam for obtaining 1 kgal distillate (distillate condensed on the tube side + condensate from steam):
0.138 ÷ (1+ 0.138) × $7/kgal = $0.85/kgal

[6] Capital recovery costs = $\dfrac{(total\ \ capital\ \ cost)\times 1000\times i\times\left[1+(i/100)\right]^{r}}{365\times(100-Dt)\times\left[(1+i/100)^{r}-1\right]}$

where r is system lifetime (yr), i is the annual interest rate (%), and Dt represents downtime (%). A system lifetime (exclusive of membrane replacement) of 15 years, an interest rate of 12%, and a downtime percentage of 15% are used as representative values.

Desalination Roadmap (2003, p. 44) indicates that the TBRDC will have testing facilities for brackish water desalination as well as necessary land resources to evaluate concentrate disposal. Fresh water source is also available. Engineering capabilities needed for plumbing and electrical connections will be locally

available. Selection of an alternate site will be undertaken in the highly unlikely event of the TBRDC not being ready or unavailable.

The manufacturer of the hollow-fiber devices for the pilot plant, AMT, is interested in larger-scale commercialization of such devices. Employing the same module frame used here, the membrane surface area can be doubled since fibers occupy only half of the depth of the module at this time. Stacking 5-6 such modules and two such stacks in parallel may yield more than 1 gpm distillate water in a pilot plant. However, additional efforts will have to be made by AMT to develop much larger membrane units for larger-scale plants. That is again part of a natural progression in the development of a technology.

5. Analysis of Results and Commercial Viability of the Project

An analysis of the results obtained in the project indicates the following:

1. The high water vapor fluxes obtained earlier from small horizontal crossflow modules containing larger diameter/thicker wall coated PP hollow fibers in Phase II are also achieved in this project using modules that have more than an order of magnitude larger membrane surface area 2,864 cm^2 (Phase III vs. 119 cm^2 in Phase II). The maximum value of the water vapor flux achieved was around 60 $kg/m^2 \cdot h$ for 87-90 °C brine feed.

2. Studies using small modules identical to those in Phase II and the smaller 50/280 μm PP fibers indicated that their DCMD performances or VMD performances were much poorer compared to those using 150/330 μm fibers. This conclusion is valid whether the fibers have a coating or not. Therefore, the hollow fibers employed here in the larger modules are the same larger diameter hollow fibers used in Phase II; however, the microporous silicone-fluoropolymer coatings on the fiber outside surface were somewhat tighter than those in Phase II. The fiber lengths employed here are four times longer than those in Phase II. The substantially increased fiber length requires greater attention to the distillate flow rate in a scaled-up configuration; otherwise distillate overheating will take place reducing the temperature driving force across the pore and therefore the water vapor flux.

3. Two rectangular hollow-fiber modules were easily stacked back-to-back to achieve 5,728 cm^2 membrane surface area so that the hot brine feed leaving one module immediately enters the next. This demonstrates that one can stack 4-6 or more modules face-to-face to extract a much greater amount of sensible heat from the same hot brine feed in sequence. The modules that are downstream will be exposed to a lower temperature brine feed. Experiments carried out demonstrate that even at a brine feed temperature as low as 60 °C, one can get a water vapor flux > 20 $kg/m^2 \cdot h$.

4. Experiments demonstrate that water vapor flux reduction due to an increase in feed salt concentration from 0-10% leads to a very limited water vapor flux reduction. This technique is useful for concentrate volume reduction and further water recovery.

5. The 5-day extended-duration experiment and many studies during the whole project did not resort to any membrane cleaning beyond a 1 μm microfilter at the module inlet. The behavior was essentially unaffected with time providing a justifiable optimistic basis for further scale-up and potential future use.

6. Conservative economic calculations demonstrate substantial economic advantages of this technique vis-a-vis RO as long as waste heat sources are available.

7. There exists a reasonable basis to go forward to a 1-5 gpm pilot plant study employing fibers and modules of the type used here in a stacked up mode. However, larger modules may be more useful for larger plants.

References

Costello, M. J., A. G. Fane, P. A. Hogan and R. W. Schofield, 1993. *The effect of shell side hydrodynamics on the performance of axial flow hollow fiber modules,* J. Membr. Sci. 80, 1-11.

Godino, M. P., L. Pena, and J. I. Mengual, 1996. *Membrane distillation: Theory and experiments,* J. Membr. Sci., 121, 83.

Gryta, M., M. Tomaszewska, A. W. Morawski, 1997. *Membrane distillation with laminar flow*, Separation and Purification Technology 11, 93-101.

Hobler, T., *Heat Transfer and Heat Exchangers*, 1986. PWN, Warsaw.

Incropear, F. P., D. P. Dewitt, 2002. *Chapter 7. External flow, in Introduction of Heat Transfer,* Fourth Edition, John Wiley & Sons, New York, pp. 363-342.

Kreith, F., M. S. Bohn, 2001. *Chapter 7. Forced convection over exterior surfaces, in Principles of Heat Transfer,* Six Edition, Brooks/Cole, Pacific Grove, CA., pp.421-483.

Lawson, K. W., and D. R. Lloyd, 1996a. *Membrane distillation, II. Direct contact MD,* J. Membr. Sci., 120, 123-133.

Lawson, K. W., and D. R. Lloyd, 1996b. Membrane distillation, I. Module design and performance evaluation using vacuum membrane distillation, J. Membr. Sci., 120, 111-121.

Lawson, K. W., D. L. Lloyd, 1997. *Membrane distillation,* J. Membr. Sci. 124, 1.

Martinez-Diez, L. and M. I. Vazquez-Gonzalez, 1996. *Temperature polarization in mass transport through hydrophobic membranes,* AIChE J. 42 (7), 1844.

Martinez-Diez, L., and M. I. Vazquez-Gonzalez, 1999. Temperature and concentration polarization in membrane distillation of aqueous salt solutions, J. Membr. Sci., 156, 265-273.

Mulder, M., 1991. *Basic Principles of Membrane Technology*, 2nd Ed., Kluwer Academic Publishers.

Pena, L., M. P. Godino, and J. I. Mengual, 1998. *A method to evaluate the net membrane distillation coefficients,* Ibid. 143, 219.

Peters, M.S. and K. D. Timmerhaus, 1991. *Plant Design and Economics for Chemical Engineers,* 4th Ed., McGraw Hill, New York.

Porter, M. C., 1972. *Concentration polarization with membrane ultrafiltration,* Ind. Eng. Chem. Prod. Res. Dev., 11, 234.

Pusch, W., 1972. Concentration polarization in hyperfiltration systems, in H.K. Lonsdale and H. E. Podall (Eds.), Reverse Osmosis Membrane Research, Plenum Press, New York, pp. 43-58.

Ray, R., 2001. *Membrane Handbook* (Eds. W. S. Ho, and K. K. Sirkar), Chapter 25, Kluwer Academic Publishers, Boston.

Schofield, R. W., A. G. Fane, and C. J. D. Fell, 1987. *Heat and mass transfer in membrane distillation,* J. Membr. Sci., 33, 299.

Schofield, R. W., A. G. Fane, and C. J. D. Fell, 1990a. Gas and vapor transport through microporous membrane. I. Knudsen-Poiseuille transition, J. Membr. Sci., 53, 159-171.

Schofield, R. W., A. G. Fane, and C. J. D. Fell, 1990b. *Gas and vapor transport through microporous membrane. II,* J. Membr. Sci., 53, 173-185.

Schofield, R. W., A. G. Fane, C. J. D. Fell, and R. Macoun, 1990c. *Factors affecting flux in membrane distillation, Desalination,* 77 (1-3), 279.

Schoner, P., P. Plucinski, W. Nitsch and U. Daiminger, 1998. *Mass transfer in the shell side of crossflow hollow fiber modules,* Chemical Engineering Science 53 (13), 2319.

Sirkar, K. K and Y. Qin, 2001. "Novel Membrane and Device for Direct Contact Membrane Distillation Based Desalination Process," Desalination Research and Development Program Report No. 87.

Sirkar, K. K and B. Li, 2003. "Novel Membrane and Device for Direct Contact Membrane Distillation-Based Desalination Process: Phase II", Desalination Research and Development Program Report No. 96.

Appendix

Data Tables

Table A1. Experimental Data Used in Figure 10. VMD: Variation of Water Vapor Flux of Modules MXFR #11, MXFR #12, MXFR #13, and MXFR #14 with Interstitial Velocity of 1% Brine as Feed Flowing Through the Shell Side at 85 ^{o}C; Tube Side at a Vacuum of 64-69 cm Hg

Interstitial Velocity, cm/min	Water vapor flux kg/m^2·h			
	MXFR#11	MXFR#12	MXFR#13	MXFR#14
43				9.676
47		11.297		
48.9	9.106		8.703	
99	10.36			11.385
102			9.901	
108		13.129		
200	11.083	13.83		
206			10.923	12.303
300	11.246	14.416		13.041
305			10.876	
374			11.154	
378	11.223	14.591		12.671

Table A2. Experimental Data Used in Figure 11. DCMD: Variation of Water Vapor Flux of Membrane Modules MXFR #11, #12, #13, #14, and #15 with Interstitial Velocity of Hot Brine (1% NaCl) as Feed Flowing Through the Shell Side at 85 ^{o}C (Tube Side: DI Water, 15-19 ^{o}C, Linear Velocity 770 cm/min)

Interstitial velocity cm/min	Water vapor flux kg/m^2·h				
	MXFR#11	MXFR#12	MXFR#13	MXFR#14	MXFR#15
57			2.096	2.514	
60	2.001	2.304			2.615
128	3.735	3.65	3.599	4.414	3.592
206	4.296				5.255
210		4.683			
217				5.437	
220			4.399		
277				5.961	
286		5.493			
294	4.9		5.12		
315					5.66
378	4.872	6.99	5.152	6.137	

Table A3. Experimental Data Used in Figure 12. Variation of Water Vapor Flux of Module S/N 1005 with Interstitial Velocity of 3% Brine Flowing Through Shell Side at a Feed Temperature of 85 °C and Distillate Entering the Tube Side with a Linear Velocity of 1,560 cm/min at 16 °C

Interstitial velocity cm/min	Water vapor flux $kg/m^2 \cdot h$
137	32.6
175	29.2
207	28.1
230	28
251	27.4
276	27.1

Table A4. Experimental Data Used in Figure 13. Comparison of DCMD Performances of Modules S/N 1004 and S/N 1005: Variation of Water Vapor Flux with Inlet Linear Velocity and Outlet Temperature of Distillate Flowing Through the Tube Side at Inlet Temperatures of 16-24 ^oC and 3% Brine at 85 ^oC Flowing on the Shell Side at 25 L/min (Interstitial Velocity of 230 cm/min)

Linear velocity cm/min	Water vapor flux $kg/m^2 \cdot h$		Outlet temperature of distillate ^oC	
	S/N 1004	S/N 1005	S/N 1004	S/N 1005
1,183	23.2		84	
1,720	35.4		83	
2,258	43.2		83	
2,795	48.1		80	
3,225	50		77	
3,548	52.6		74	
3,871	54.1		74	
1,226		22.9		84
1,716		33.2		83.5
2,044		36.71		81.5
2,338		39.8		78.5
2,853		43.5		76
3,118		46		71.4
3,310		45.7		70.9
3200		45.2		71

Table A5. Experimental Data Used in Figure 14. DCMD Performance of Module S/N 1004 (Membrane Surface Area: 2,864 cm^2) with City Water, 3% Brine, 6% Brine, and 10% Brine as Feed Solutions: Variation of Water Vapor Flux with Feed Inlet Temperature (Shell Side: Brine Solution at 230 cm/min of Interstitial Velocity; Tube Side: Distillate at 2,850 cm/min of Average Linear Velocity at 25-35 ^oC of the Inlet Temperature)

Brine inlet temperature ^oC	City water	3% NaCl	6% NaCl	10% NaCl
	Water vapor flux $kg/m^2 \cdot h$			
40	4.16	5.23	3.47	4.3
50		9.31	9.9	9.06
60	17.56	17.3		18.47
61.9			18.91	
70	29.41	28.9	26.77	27.34
80	41.46	40.78	41.3	43.72
83.5			45.6	
85	47.6	47.8		47.4
90	52.82	52.8	53.2	50.21
93	55.6	54.5	55.7	55.1

Table A6. Experimental Data Used in Figure 15. DCMD Performance of Module S/N 1004 (Membrane Surface Area: 2,864 cm^2) with 3% Brine and 10% Brine as Feed Solutions: Variation of Water Vapor Flux with Linear Velocity of Distillate Flowing Through Tube Side at Inlet Temperatures of 18-26 °C and Hot Brine Flowing on Shell Side with 25 L/min (Interstitial Velocity of 230 cm/min) at a Temperature of 85-88 °C

Linear velocity cm/min	3% NaCl	10% NaCl
	Water vapor flux $kg/m^2 \cdot h$	
1,183	23.2	23.3
1,666		34.5
1,720	35.4	
2,258	43.2	
2,354		42.3
2,795	48.1	
2,913		52.7
3,225	50	
3,360		50.3
3,548	52.6	
3,659		51.1
3,871	54.1	
4,003		52.7

Table A7. Experimental Data Used in Figure 16. DCMD Performance of Module S/N 1004 (Membrane Surface Area: 2864 cm^2): Variation of Water Vapor Flux with Distillate Inlet Temperature (Shell Side: 3% Brine at 230 cm/min of Interstitial Velocity at a Temperature of 91-93 ^oC; Tube Side: Distillate at 2,950 cm/min of Linear Velocity); Variation of Distillate Outlet Temperature with the Distillate Inlet Temperature has also Been Shown

Distillate inlet temperature ^oC	Water vapor flux $kg/m^2 \cdot h$	Distillate outlet temperature ^oC
44	45.32	89
50	42.02	90.5
55	37.05	91.5
60	26.31	92
36.1	52.27	88.3
32.8	56.56	87.92
40.1	48.88	89.6

Table A8. Experimental Data Used in Figure 17. DCMD: Variation of Water Vapor Flux with Operating Time for Hot Brine (3% NaCl) Recirculating Through the Shell Side with an Inlet Velocity of 253 cm/min (Reynolds Number, 78) at 87-90 ^{o}C, and Cold Distillate Water Recirculating Through Tube Side at an Inlet Velocity of 3,870-4,060 cm/min (Reynolds Number, 448-471) at an Inlet Temperature of 34-42 ^{o}C (Module: S/N 1004)

Operation time hr	Water vapor flux kg/m^2·h
2	57.61
7.5	56.46
9.5	60.47
11	59.3
25.5	54.92
27.5	54.62
30.5	52.4
32.5	54.05
35.5	57.15
49.5	58.15
51.5	50.42
54.5	55.98
57	56.63
59.5	58.4
74	59.62
76	54.09
78.5	54.8
80.5	57.48
83.5	56.01
102.5	56.74
104.5	50.2
105.5	51.86
106.5	51.05
108.5	52.37
122.5	65.85
123.5	53.63
124.5	55.52
127.5	49.7

Table A9. Experimental Data Used in Figure 18. Variation of Water Vapor Flux of Stacked Modules S/N 1004 (Outlet) and S/N 1005 (Inlet) (Total Membrane Surface Area: 5,728 cm^2) with Inlet Temperature for 3% Brine as Feed Flowing Through Shell Side at an Interstitial Velocity of 230 cm/min and Distillate Flowing on the Tube Side with a Linear Velocity of 3,000 cm/min at Inlet Temperatures from 24-50 ^{o}C

Brine feed temperature (inlet) ^{o}C	Water vapor flux kg/m^2·h
42	4.24
49	6.54
61	14.33
70.5	21.51
74	23.08
78	27.67

Table A10. Experimental Data Used in Figure 19. Variation of Water Vapor Flux of Stacked Modules S/N 1004 (Outlet) + S/N 1005 (Inlet) with Interstitial Velocity of 3% Brine Flowing Through the Shell Side at Inlet Temperatures from 81-75 ^{o}C and Distillate Flowing on the Tube Side with a Linear Velocity of 3,120 cm/min at Inlet Temperatures from 28-50 ^{o}C

Interstitial velocity cm/min	Water vapor flux $kg/m^2 \cdot h$
92	24.9
138	26
184	26.4
230	25.4
253	25.8
276	25.9